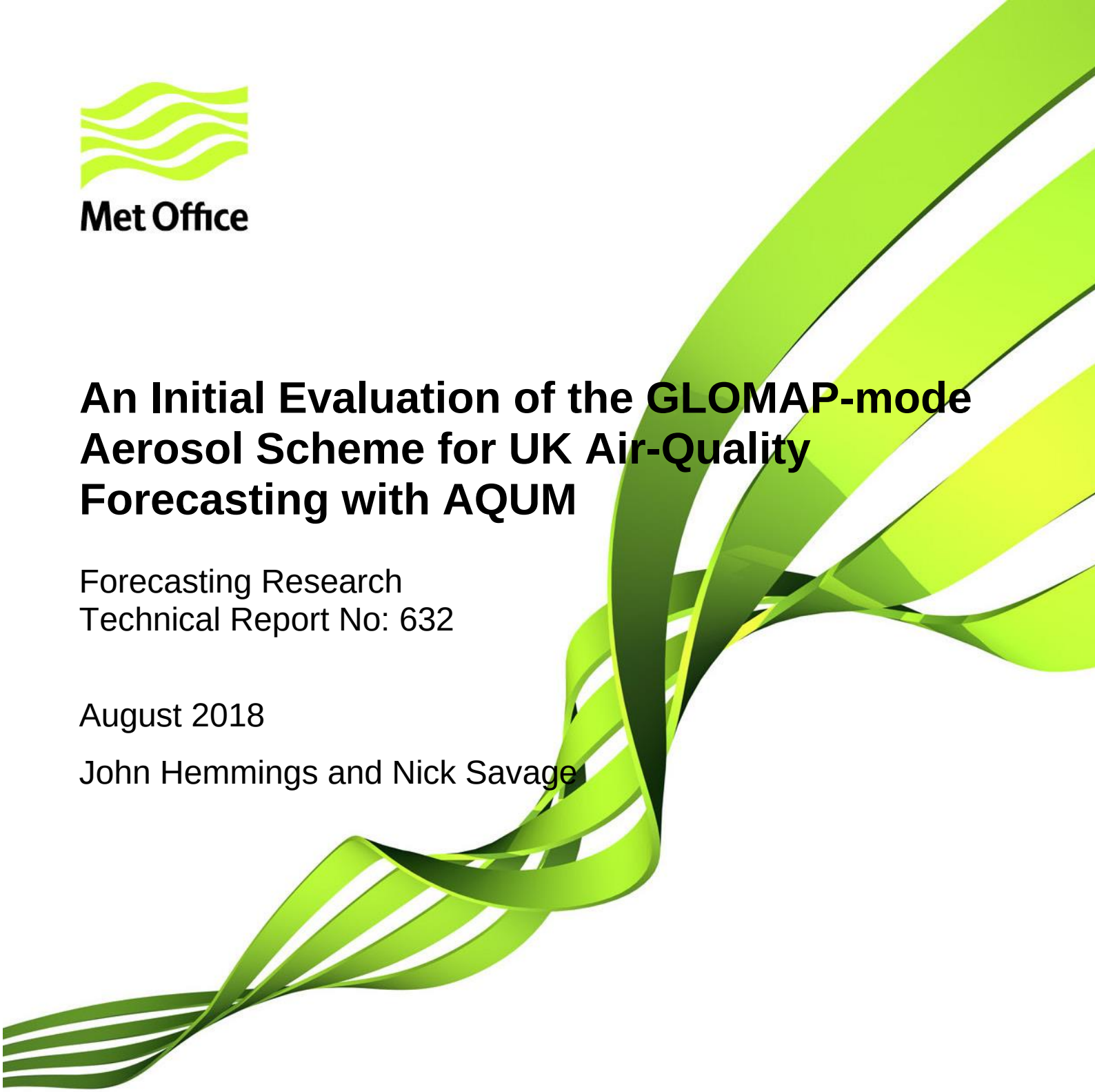

An Initial Evaluation of the GLOMAP-mode Aerosol Scheme for UK Air-Quality Forecasting with AQUM

Forecasting Research
Technical Report No: 632

August 2018

John Hemmings and Nick Savage

Contents

Executive Summary

The current AQUM forecast system for UK air quality uses the UKCA community model to represent gas phase chemistry but relies on the older CLASSIC model to simulate aerosol processes. An alternative would be to use the GLOMAP-mode aerosol scheme that is an integral part of UKCA. An initial evaluation of GLOMAP-mode as a potential replacement for the main elements of CLASSIC is presented, focussing on the likely impact on pollutant species affecting the Daily Air Quality Index product: ozone (O_3), nitrogen dioxide (NO_2), sulphur dioxide (SO_2), $PM_{2.5}$ and PM_{10}. Replacement of the CLASSIC dust scheme is not considered.

At present, GLOMAP-mode does not have a nitrate scheme suitable for operational use. The dominance of ammonium nitrate in many UK pollution episodes dictates that such a scheme is essential before the use of GLOMAP-mode could be considered for the UK forecast. A further evaluation would therefore be required once nitrate is included.

GLOMAP-mode differs from CLASSIC in providing a more sophisticated treatment of the aerosol and including a prognostic scheme for sea salt that allows its contribution to PM over land to be represented. The configuration of GLOMAP-mode evaluated here models the aerosol in the form of 5 internally mixed 'modes' with dynamically-evolving size spectra. These represent 4 size categories of soluble material (comprising sulphate, black carbon, organic carbon and sea salt) and one of insoluble material (comprising black carbon and organic carbon). This contrasts with CLASSIC, where the non-dust aerosol is represented by 5 independently transported species (ammonium nitrate, ammonium sulphate, fossil fuel black carbon, fossil fuel organic carbon and biomass burning aerosol), each with 2 or 3 fixed size spectra accounting for different forms, and a climatological secondary organic aerosol field. GLOMAP-mode also models the number concentration of aerosol in each mode separately from its mass, allowing for a better representation of microphysical processes such as nucleation.

GLOMAP-mode is supported by an extension to UKCA's Regional Air Quality (RAQ) scheme used for gas phase chemistry in AQUM. The extension provides an alternative model of aerosol precursor chemistry to that used in CLASSIC. Additionally, unlike AQUM-CLASSIC, the GLOMAP-mode configuration does not include chemistry on

aerosol surfaces or any feedback to the meteorology with respect to the aerosol. The absence of a direct aerosol effect is compensated for by including the radiative effect of climatological aerosol profiles in the troposphere, rather than in the stratosphere only as done for AQUM-CLASSIC.

The evaluation is based on a comparison of 2015 case-study output between the present AQUM-CLASSIC configuration and an AQUM-GLOMAP configuration in which GLOMAP-mode and the RAQ scheme extension have been substituted for the non-dust components of CLASSIC with minimal changes to other elements of the system. Required changes included the adaptation of emissions and lateral boundary conditions to accommodate the different aerosol representation. A further modification, exploiting UKCA's common framework for gas and aerosol emissions, was the matching of temporal and vertical patterns of aerosol and aerosol precursor species emissions to those used for gaseous species from the same anthropogenic sources.

The key findings, based primarily on performance statistics for UK sites with time series of surface observations, are as follows.

- The performance of AQUM-GLOMAP for O_3 and NO_2 shows only minor differences from AQUM-CLASSIC in the form of small concentration increases. These are attributable to the omission of chemistry on aerosol surfaces in the present AQUM-GLOMAP configuration.

- Concentrations of SO_2 tend to be a little higher on average in AQUM-GLOMAP than in AQUM-CLASSIC, causing notably larger spring and summer biases, but remain well below the threshold required to register on the DAQI.

- Concentrations of $PM_{2.5}$ are much lower in AQUM-GLOMAP than in AQUM-CLASSIC, increasing a tendency towards negative bias in winter and spring and introducing negative biases in summer and autumn. Less than half of this reduction is likely to be due to the absence of a nitrate contribution. An analysis of sulphate contributions from different size categories in each configuration suggests that at least part of the remainder can be attributed to a tendency towards larger particles in AQUM-GLOMAP, increasing deposition losses.

- $PM_{2.5}$ is less well correlated with observations in AQUM-GLOMAP than in AQUM-CLASSIC but this aspect of performance degradation seems to be primarily due to the absence of a nitrate scheme.

- Winter-time concentrations of PM_{10} are much greater in AQUM-GLOMAP than in AQUM-CLASSIC and the magnitude of negative biases are reduced in all seasons. This is attributable to the introduction of the prognostic sea-salt aerosol that more than compensates for any increases in negative bias due to the absence of a nitrate contribution. The bias reduction leaves scope for further reductions to be achieved by the introduction of a nitrate scheme.

- Despite reducing the PM_{10} bias, sea-salt has a detrimental effect on the correlation between the model output and observations. The effect is particularly dramatic in winter when all correlation is lost, severely compromising any improvements in predictive skill. However, the frequency distribution of PM_{10} and the characteristics of its temporal variability seem to be better represented. A more thorough investigation will be required to resolve the causes of the detrimental effects and determine how they might be reduced by configurational changes and/or by modifications to the sea-salt scheme.

- Run times for AQUM-GLOMAP were typically 40-50% longer than AQUM-CLASSIC, although this increase may be alleviated to some extent by developments currently in progress to improve the efficiency of the aerosol code.

The present study serves as a proof of concept, demonstrating the feasibility of replacing CLASSIC with GLOMAP-mode, conditional on the availability of a suitable nitrate scheme. However, the detrimental impact on the $PM_{2.5}$ bias and PM_{10} correlation statistics are a cause for concern that must be satisfactorily addressed prior to any operational use. Other priority improvements to consider are the inclusion of direct and indirect aerosol feedbacks to the meteorology, using available schemes in UKCA, and the inclusion of secondary organic aerosols, both biogenic that are currently supported in UKCA and anthropogenic that are not. The greater sophistication of GLOMAP-mode and its status as a community model under active development gives it great potential to improve PM forecasts in the future but considerable effort will still be required before it can replace CLASSIC in routine operational forecasting.

1. Introduction

The AQUM forecasting system currently uses the UKCA model (Morgenstern et al., 2009, O'Connor et al., 2014) to represent gas phase chemistry and the CLASSIC model (Bellouin et al. 2011) to represent aerosol processes. One of the priority areas for future development identified in an initial evaluation of AQUM by Savage et al. (2013) is the replacement of the CLASSIC aerosol scheme by the GLOMAP-mode scheme (Mann et al., 2010, 2012) which is an integral component of UKCA. GLOMAP-mode is a relatively new size-resolved aerosol microphysics model developed by the UKCA community which represents the aerosol in terms of both mass and number concentrations. The scheme offers a much more sophisticated treatment of the aerosol than CLASSIC, including the time evolution of the size spectra associated with different aerosol modes, the representation of internally mixed particles, the inclusion of microphysical processes such as nucleation and an improved coupling with UKCA oxidants. In addition, the GLOMAP-mode scheme would allow the contribution of sea-salt to the aerosol to be represented over the whole of the UK, whereas in CLASSIC sea-salt aerosol is not transported over land.

The purpose of this initial evaluation is to assess the potential of GLOMAP-mode for UK air quality forecasting in the AQUM system and to start to identify areas where further investigation or development might be required prior to any operational deployment. Section 2 gives a brief overview of the CLASSIC and GLOMAP-mode aerosol schemes and the key differences between them. The method for the evaluation experiment is given in Section 3. Section 4 presents the findings and these are summarised with some conclusions in Section 5.

2. Aerosol Schemes

The descriptions of the schemes here relate to the configurations used in the evaluation experiment. In particular, it should be noted that the version of GLOMAP-mode being considered for implementation in AQUM does not include dust and that dust is modelled identically in both configurations using the CLASSIC dust scheme.

2.1 CLASSIC

CLASSIC is a bulk aerosol scheme in which 6 advected species are transported independently with the prognostic variables being the mass of each, partitioned between up to 3 tracers that represent different modes for each species as shown in Figure 1. Ammonium nitrate, ammonium sulphate, fossil fuel black carbon, fossil fuel organic carbon and aerosols from biomass burning are assumed to have fixed log-normal size distributions for each mode and mineral dust is represented by 6 size bins. There are 20 advected tracers in all. Sea-salt in two size classes is represented by diagnostic concentrations over the open ocean only (and not advected) and biogenic secondary organic aerosol (SOA) is represented by a 3-D climatology. Sulphur chemistry for modelling aerosol precursor species is included, adding another 3 tracers, sulphur dioxide (SO_2), dimethyl sulphate (DMS) and ammonia (NH_3) to give a total of 23.

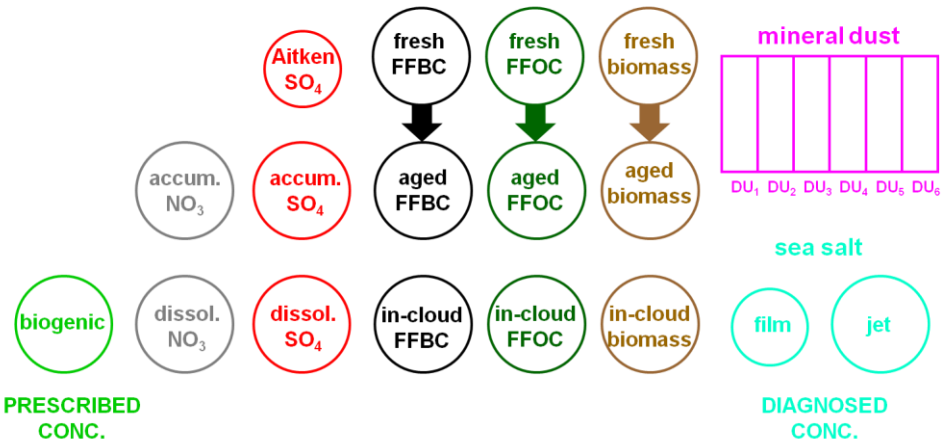

Figure 1. Aerosol representation in the CLASSIC scheme. (See text for details.) Adapted from original material by Graham Mann, University of Leeds.

Emissions of primary aerosols in AQUM comprise surface and high-level emissions of black carbon (BC) and organic carbon (OC) from fossil fuel burning and aerosols from biomass burning (a combination of BC and OC) with emissions distributed over a range of model levels. Emissions of aerosol precursor species comprise surface and high-level

emissions of SO_2 and surface emissions of NH_3, together with natural emissions of SO_2 from volcanic activity from a 3-D climatology and marine DMS emissions. Anthropogenic emissions are derived from annually updated data provided by the UK National Atmospheric Emissions Inventory (NAEI) and the European Monitoring and Evaluation Programme inventory, together with shipping emissions based on the ENTEC inventory available for 2007.

Aerosols interact with the gas phase chemistry in AQUM via a heterogeneous chemistry scheme that accounts for the hydrolysis of dinitrogen pentoxide (N_2O_5) on some of the CLASSIC aerosol particles. They also interact with gas phase chemistry via two-way coupling of the following oxidant fields: ozone (O_3), hydrogen peroxide (H_2O_2), hydroxyl radical (OH) and hydroperoxl radicals (HO_2). These fields from UKCA are passed into CLASSIC and used in the oxidation of SO_2 and DMS. The resulting changes are passed back into UKCA after the CLASSIC chemistry call. Changes in nitric acid (HNO_3) from its equilibrium with NH_3 forming ammonium nitrate (NH_4NO_3) are also applied to UKCA's HNO_3 concentrations.

Aerosols in AQUM are fully coupled with the meteorology with the direct effect on radiation and the indirect effects on cloud droplet formation and precipitation included.

2.2 GLOMAP-mode with CLASSIC Dust

The AQUM configuration being evaluated will be referred to as AQUM-GLOMAP. It comprises GLOMAP-mode MS2, coupled with the RAQ-Aero chemistry scheme, an extended version of the Regional Air Quality or RAQ scheme used with CLASSIC in the operational AQUM system. In the MS2 setup of GLOMAP-mode, the aerosol is represented by 5 internally-mixed log-normal modes shown in Figure 2 (soluble nucleation mode, soluble Aitken mode, insoluble Aitken mode, soluble accumulation mode and soluble coarse mode). These are composed of varying amounts of sulphate (in the form of sulphuric acid), organic carbon (in the form of organic material with a fixed OM:OC ratio), black carbon and sea salt. The organic carbon component can include secondary aerosol. However, this is dependent on emissions of monoterpene which are currently omitted, so SOA which contributes to $PM_{2.5}$ and PM_{10} in CLASSIC is not represented. The prognostic tracers are the number mixing ratios for each mode, in particles per molecule of air, and the mass of each component in each mode (20 tracers

in total). The geometric mean dry diameter is allowed to vary for each mode over a prescribed size range before particle number and mass are transferred between modes. Dust is modelled separately using the CLASSIC scheme (6 tracers). The RAQ-Aero chemistry scheme introduces 8 gas phase tracers not present in RAQ (SO_2, H_2SO_4, MSA, DMS, DMSO, NH_3, monoterpene and secondary organics) giving a total requirement of 34 tracers associated with the aerosol, 11 more than for CLASSIC. GLOMAP-mode does not currently include a nitrate scheme suitable for operational use. This is a significant limitation which compromises its application to air quality forecasting for the UK where ammonium nitrate is a significant pollutant contributing to $PM_{2.5}$ and PM_{10}.

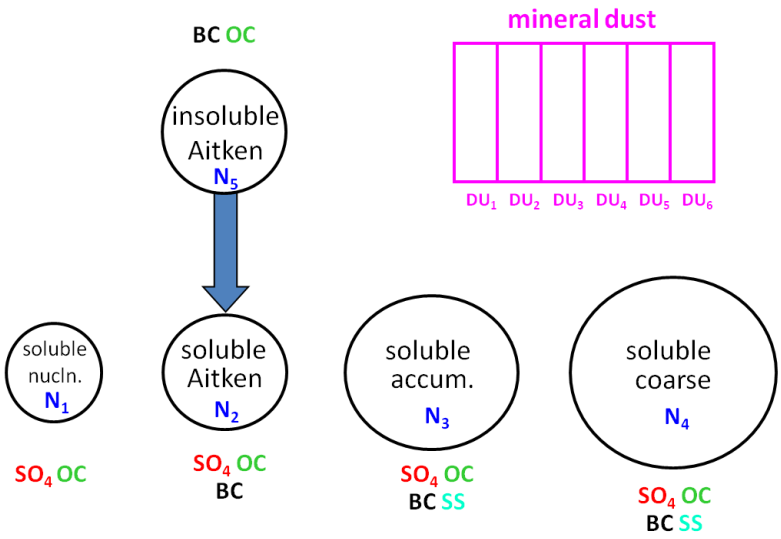

Figure 2. Aerosol representation in the GLOMAP-mode MS2 scheme with CLASSIC dust. (See text for details.) Adapted from original material by Graham Mann, University of Leeds.

For GLOMAP, the emissions of BC, OC, SO_2 and NH_3 are derived from the same data sets as used in the standard AQUM configuration with CLASSIC. (NH_3 is included with the extension of the RAQ chemistry scheme to RAQ-Aero, but is not involved in aerosol formation). Volcanic SO_2 emissions are not currently included. With that exception, the amount of material emitted for each species is the same as in CLASSIC, with the caviat that 2.5% of SO2 emissions are treated as primary sulphate aerosol in GLOMAP. Emissions of DMS are calculated online using the same DMS seawater concentration

data set as CLASSIC but GLOMAP is configured to use the Liss and Merlivat (1986) scheme for the air-sea flux calculation, as used in the global GA7 configuration, instead of the Wanninkhof (1992) scheme used in CLASSIC. GLOMAP differs from CLASSIC in modelling sea-salt emissions explicitly, rather than diagnosing boundary level sea-salt concentrations over the ocean.

Material from biomass burning is not modelled separately from the other carbonaceous aerosol tracers in GLOMAP, so biomass burning emissions must be divided between black carbon and organic carbon components. 8.75% of material is assumed to be in the form of black carbon, consistent with the ratio that CLASSIC assumes for the transported fresh material.

The vertical distribution of the anthropogenic aerosol scheme emissions varies depending on their source as defined by the Selected Nomenclature for sources of Air Pollution (SNAP) sector by which they are classified. This is enabled by functionality included in UKCA's emission system. It overcomes the limitation in CLASSIC where all emitted material must be divided between the surface level and a single high level and allows the vertical profiles of the emissions to be fully consistent with those of the RAQ gas phase emissions from the same sources. Similarly, SNAP-sector dependent daily and weekly cycles consistent with the RAQ emissions are applied, whereas in CLASSIC, although daily and weekly cycles are applied to surface emissions of fossil fuel carbon and SO_2 these are not SNAP-sector specific.

The evaluated configuration in this baseline study does not include heterogeneous chemistry or any feedback to the meteorology with respect to the GLOMAP aerosols (i.e. non-dust aerosol). It should be stressed that GLOMAP does support direct and indirect aerosol effects but that this functionality is not used in our initial GLOMAP-AQUM configuration. To compensate for this, the radiative effect of a climatological background aerosol throughout the atmosphere is included by applying the full Cusack scheme (Cusack et al., 1998) instead of just its stratospheric component which is used with CLASSIC. The Cusack scheme is based on fixed profiles for aerosol species over land and oceans.

2.3 Differences in Representation of Particulate Matter

Aerosol pollution is characterised by its contribution to airborne particulate material in the size range less than 10 µm (PM_{10}) because of the effect of these smaller particles on human health. Particulate material smaller than 2.5 µm ($PM_{2.5}$), which has the greatest potential to penetrate deep into the lungs, is considered particularly dangerous and quantified separately as a component of PM_{10}.

The most obvious difference between the PM representation in the two aerosol schemes is in the species that contribute to the total PM. Sea-salt in CLASSIC is not advected so is zero everywhere over land. It is therefore a missing contribution at all observation sites. In GLOMAP, sea-salt is represented everywhere but the absence of ammonium nitrate is expected to be a significant source of negative bias in PM estimates. In addition, the sulphate contribution to PM differs between schemes. In CLASSIC, it is in the form of ammonium sulphate ($[NH_4]_2SO_4$) whereas in GLOMAP it is in the form of sulphuric acid (H_2SO_4), having not been neutralised by NH_3. This means that 1 mole of sulphate is associated with 132 g of dry aerosol in CLASSIC but only 98 g of dry aerosol in GLOMAP.

The way in which water content of the aerosol is treated differs between the aerosol schemes and is potentially significant with respect to the diagnosed PM. $PM_{2.5}$ and PM_{10} are effectively defined by their measurement methods, rather than being completely unambiguous physical or chemical properties (AQEG, 2012). The reference method involves pumping ambient air through a size-selective inlet followed by a filter. Thus, because water content affects particle size it also affects the fraction of material contributing to each PM type. The mass deposited on the filter is measured under controlled conditions designed to constrain the quantity of water in the collected PM. Measurement is made after a conditioning period with temperature in the range 19-21C and relative humidity in the range 45-55%.

In both schemes, the mass considered is the mass of dry aerosol but there are subtle differences between the two schemes in the way that material is selected by size that can introduce significant differences in PM between the schemes even when the aerosol has broadly equivalent component concentrations and size distributions. The potential for this will depend on ambient conditions. In CLASSIC, fixed log-normal distributions are

used to determine the size fractions for $PM_{2.5}$ and PM_{10}. These distributions correspond to assumed size distributions for the dry aerosol. The larger modes with high water content (dissolved nitrate and sulphate and in-cloud carbonaceous aerosol) do not contribute any material to the diagnosed PM. In GLOMAP, the water content of the aerosol is modelled explicitly in all modes and the variable wet diameter of each mode is used to define the log-normal distribution for determining the mass fraction. This more faithfully reproduces the measurement method. It can reduce the size fractions selected for a given dry aerosol size spectrum, thus reducing the diagnosed PM. The effect will depend on the amount of water contained in the modes that contribute to the PM. In CLASSIC, only the smaller modes of each aerosol species contribute but for these the PM could be over-estimated if the water content is significant. However, the omission of any dry mass associated with the largest modes will tend to compensate for over-estimation of PM from the smaller modes. The dry mass fraction that should contribute is reduced as the water content increases so the effect again depends on conditions. As a final note, the diagnostics for both schemes will have an underlying tendency to underestimate PM when the residual water content of the measured particulate under standard conditions is significant. In a US study, where $PM_{2.5}$ measurements were made at a lower relative humidity of approximately 35%, water was found to contribute 16% of the measured PM mass in the summer, and 8% in the winter (Rees et al., 2007).

Other differences between schemes will mean that the simulated aerosol will not necessarily have broadly equivalent component concentrations and size distributions between the two. As well as the differences already noted in Section 2.2, this includes differences in the way emissions are handled and differences in the representation of aerosol processes. Further details of the CLASSIC scheme can be found in the Unified Model documentation paper UMDP020. Details of GLOMAP-mode and the RAQ and RAQ-Aero chemistry schemes are given in UMDP084.

3. Method

The GLOMAP evaluation presented here is based on an 11 month case study with a control simulation using the CLASSIC scheme and a test simulation using the GLOMAP-mode scheme with CLASSIC dust. Case studies were set up using adapted versions of the standard AQUM case study suite at PS39 (Met Office Science Repository Service suite IDs u-an309 and u-an342 for the control and test runs respectively). Each case

study requires input data sets for emissions, lateral boundary conditions (LBCs) and meteorology. The met data is in the form of daily start dumps with a validity time of 1800Z, required for initialising 30 hour forecast simulations that span each day of the run period. The chemical and aerosol fields are initialised by transplanting in data from the previous day's forecast at T+24h. A start dump containing all chemistry and aerosol fields is required for initialisation of the air quality model at the start of the case study (cold starts).

To avoid unnecessary differences between control and test runs, the same meteorology data was used for both and the LBCs for all tracers common to both schemes were identical. The same approach was used for chemistry fields in the start dump. For the test run, an AQUM-GLOMAP start dump was generated from the standard AQUM dump used in the control run. The new GLOMAP-mode aerosol fields in this dump were set to zero, the RAQ-Aero fields for SO_2, DMS and NH_3 were copied from the CLASSIC fields with appropriate unit conversion and the remaining RAQ-Aero fields not present in RAQ were set to zero. The most recent available emissions data (from 2014) were used for both simulations with differences in emissions processing for GLOMAP as described in Section 2.2.

Lateral boundary conditions (LBCs) for both simulations were derived from output of ECMWF's C-IFS forecast model, as is done in the operational AQUM forecast system. This required the development of a novel method that allows us to create GLOMAP-mode aerosol LBCs from the set of C-IFS fields already used to generate CLASSIC LBCs, extended to include sea-salt in 3 size bins. Like CLASSIC, C-IFS uses a bulk aerosol representation that does not include information relating to particle number concentrations. To solve this problem, the new method uses size distributions that have previously been associated with the C-IFS aerosol species to derive particle size distributions from the available C-IFS mass mixing ratios. In the case of soluble or hydrophilic material, number and mass defined by these distributions are then partitioned between the 4 soluble modes represented in GLOMAP according to the boundaries prescribed by GLOMAP for each mode's geometric mean diameter. In the case of hydrophobic material, they are allocated to the insoluble Aitken mode. The mass of each component is conserved in the conversion from C-IFS to GLOMAP (as it is in the much simpler conversion from C-IFS to CLASSIC) and the particle number implied by the assumed size distributions is conserved where possible, subject to GLOMAP

constraints. For sulphate, black carbon and organic carbon, the size distributions employed are those used by Reddy et al. (2005). For sea-salt, we treat each bin separately and within each bin, a size distribution corresponding to the appropriate log-normal mode from O'Dowd et al. (1997) is used. Further details are given in a document entitled 'Method for Conversion of C-IFS Aerosol Tracers to GLOMAP-mode Tracers in AQUM Lateral Boundary Conditions'. This is included in the Supplementary Material section at the end of this report.

The standard suite uses archived LBCs from previous AQUM runs together with start dumps from these runs that provide daily UM met data. The latter also provide chemistry and aerosol data for cold starts at the beginning of the case study period. This method is unsuitable for GLOMAP case studies which require bespoke LBCs generated from the original C-IFS fields. Conversion of standard AQUM LBC files is not an option because of the absence of sea-salt data. An alternative method was therefore used for the GLOMAP evaluation experiment and applied to both the control and test runs to minimise differences between them.

The alternative method makes use of a "re-run" archive of LBCs and start dumps for the standard AQUM configuration that had been created previously to allow year-long case studies to be performed for the 2015 calendar year in the absence of archived files compatible with the current UM version. (Previously archived files were incompatible as a consequence of the replacement of New Dynamics with ENDGAME in March 2016, at OS37.) The re-run archive differs from the archive used for the standard AQUM configuration in using ECMWF meteorology data in place of data from the UM. The associated ECMWF meteorology and chemistry files were readily available for generating 2015 GLOMAP LBCs having been retrieved for creation of the re-run archive. The chemistry files contain C-IFS model forecast data at 80 km resolution and the meteorology files contain IFS forecast data, also at 80 km. It should be noted that unlike the LBCs used operationally, those used here do not include any bias corrections for ozone. In operational runs, ozone corrections are applied based on a comparison between the ECMWF output and surface observations at all remote and rural AURN sites.

The run period for the case studies was from 1800Z on 31st December 2014 to the end of November 2015. The run was initialized from a re-run archive start dump with the

correct time of validity. The performance of the model with the two different aerosol schemes is compared with a particular focus on the representation of pollutants affecting the Daily Air Quality Index (DAQI), the primary forecast product. DAQI pollution levels are given in Table 1 for reference.

Table 1. Daily Air Quality Index

DAQI	Ozone ($\mu g\ m^{-3}$) Running 8 Hourly mean	Nitrogen Dioxide ($\mu g\ m^{-3}$) Hourly mean	Sulphur Dioxide ($\mu g\ m^{-3}$) 15 minute mean	$PM_{2.5}$ Particles ($\mu g\ m^{-3}$) 24 hour mean	PM_{10} Particles ($\mu g\ m^{-3}$) 24 hour mean
1	0-33	0-67	0-88	0-11	0-16
2	34-66	68-134	89-177	12-23	17-33
3	67-100	135-200	178-266	24-35	34-50
4	101-120	201-267	267-354	36-41	51-58
5	121-140	268-334	355-443	42-47	59-66
6	141-160	335-400	444-532	48-53	67-75
7	161-187	401-467	533-710	54-58	76-83
8	188-213	468-534	711-887	59-64	84-91
9	214-240	535-600	888-1064	65-70	92-100
10	241 +	601 +	1065 +	71 +	101 +

4. Results

4.1 Evaluation for Gaseous Pollutants

The performance of AQUM-GLOMAP is first examined for the gaseous pollutants: ozone (O_3), nitrogen dioxide (NO_2) and sulphur dioxide (SO_2). SO_2 is of relatively minor importance, since DAQI limits for SO_2 are exceeded much less often than for the other two gases. Figures 3-5 show seasonal comparisons of the performance of test (AQUM-GLOMAP) and control (AQUM-CLASSIC) runs against the set of observations at Automatic Urban and Regional Network (AURN) sites distributed across the UK for each pollutant. O_3 and NO_2 observations are both represented by measurements at 70 sites. SO_2 observations are taken from 20 sites. Larger biases are present for O_3 and NO_2 than would normally be seen in operational runs because of the omission of bias corrections in the ozone LBCs from the re-run archive.

Figure 3 shows only minor differences in O_3 between the control and test simulations. However there is a very slight increase in O_3 levels in the GLOMAP test run which is consistent across all seasons as indicated by the higher bias values in Table 2. The difference in seasonal bias varies from about 0.4 µg m^{-3} in winter to about 1.4 µg m^{-3} in summer. A similar but more obvious difference in NO_2 levels is seen in Figure 4, helping to correct the negative bias present over all seasons, with the magnitude of the bias reduction (deduced from Table 3) ranging from about 0.9 µg m^{-3} in autumn to about 1.8 µg m^{-3} in winter. These small increases in NO_2 and O_3 seem consistent with the absence of heterogeneous chemistry in the GLOMAP run implying no hydrolysis of N_2O_5 on aerosol particles. The inclusion of this reaction in AQUM has previously been shown to reduce NO_2 and lead to a small reduction in positive O_3 biases during spring and summer (Ordóñez et al. 2015). The correlation coefficients with respect to observations for O_3 and NO_2 (Tables 2 and 3) are almost identical between control and test runs showing no significant change in the model's ability to reproduce the patterns in the observational data.

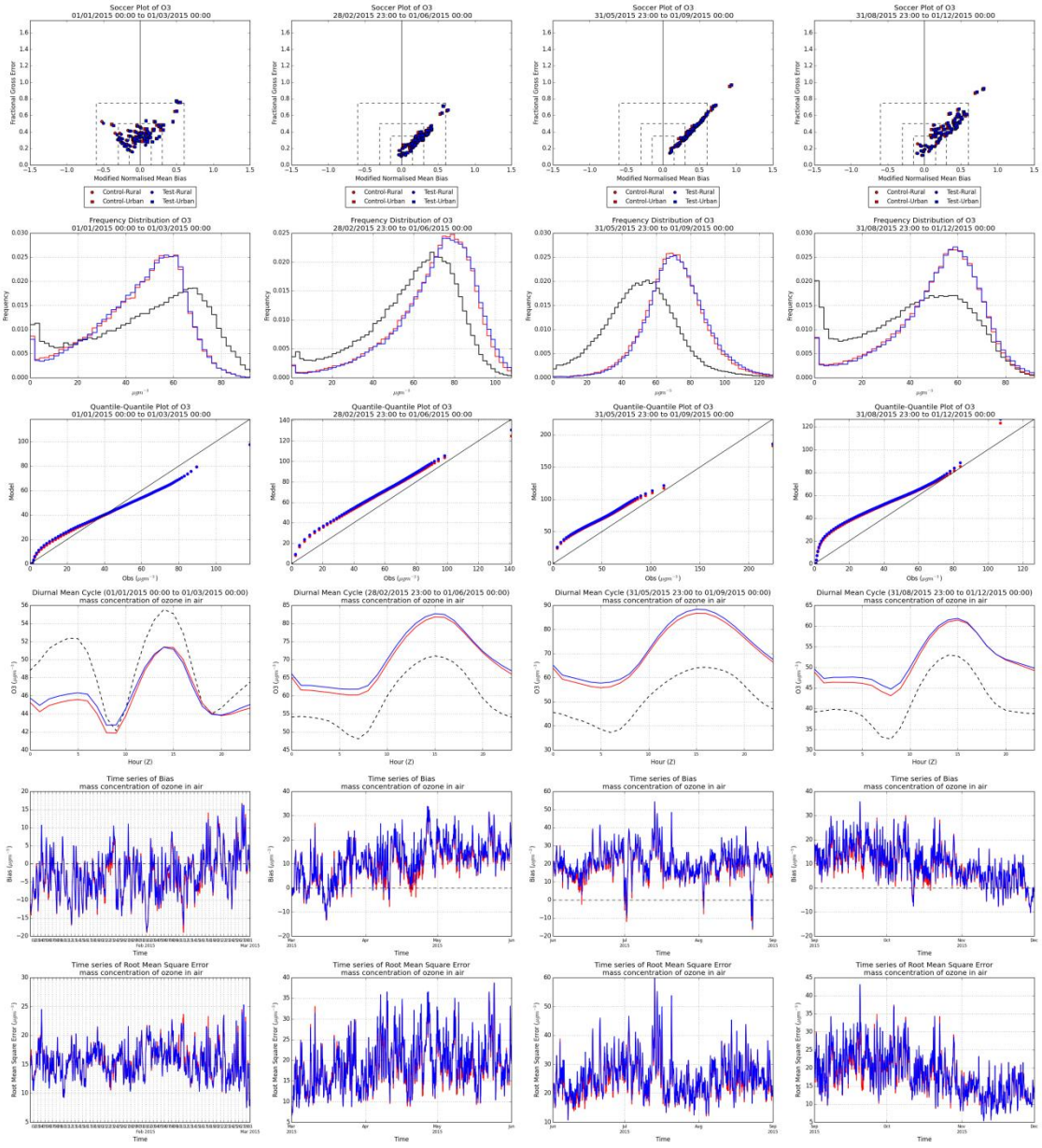

Figure 3. Statistical summaries of performance by meteorological season for O_3, for the control run (red) and the test run (blue). Observational frequency distributions and mean diurnal cycles are included for reference (black). Seasons from left to right are winter (represented by January and February only), spring, summer and autumn.

Table 2. Seasonal performance metrics for O_3

Statistic	Period	Control	Test
Correlation	JF	0.76	0.76
	MAM	0.70	0.70
	JJA	0.64	0.65
	SON	0.70	0.69
Bias (µg m^{-3})	JF	-3.27	-2.90
	MAM	10.37	11.42
	JJA	19.07	20.48
	SON	9.25	10.03
RMSE (µg m^{-3})	JF	15.76	15.66
	MAM	19.29	19.89
	JJA	25.66	26.66
	SON	18.64	19.15

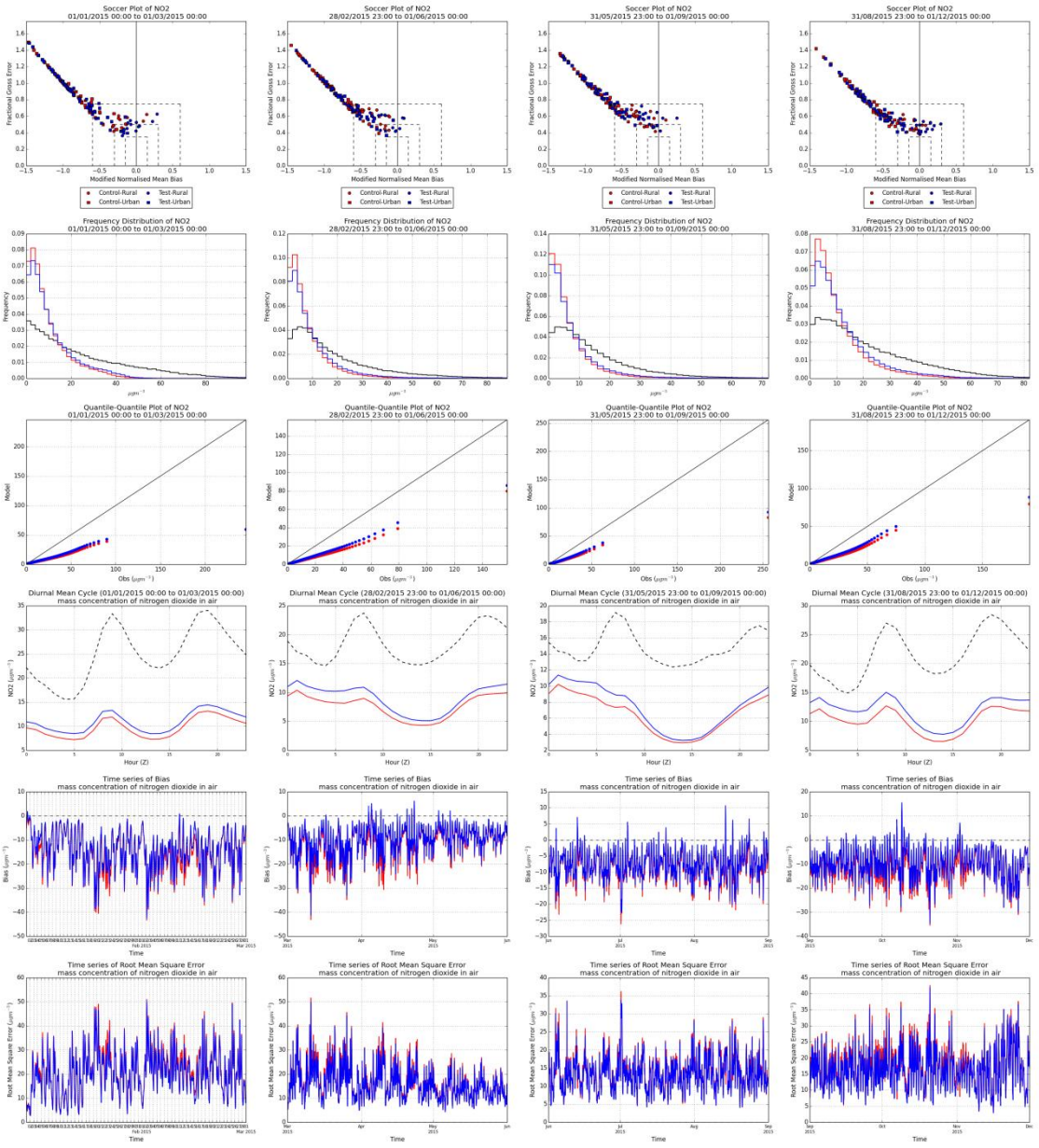

Figure 4. Statistical summaries of performance by meteorological season for NO_2, for the control run (red) and the test run (blue). Observational frequency distributions and mean diurnal cycles are included for reference (black). Seasons from left to right are winter (represented by January and February only), spring, summer and autumn.

Table 3. Seasonal performance metrics for NO_2

Statistic	Period	Control	Test
Correlation	JF	0.68	0.67
	MAM	0.60	0.59
	JJA	0.50	0.49
	SON	0.59	0.58
Bias (µg m^{-3})	JF	-15.24	-13.96
	MAM	-10.98	-9.56
	JJA	-8.24	-7.36
	SON	-11.28	-9.52
RMSE (µg m^{-3})	JF	22.82	21.86
	MAM	17.83	16.94
	JJA	14.36	13.95
	SON	18.20	17.30

Figure 5 shows rather more marked differences between the test and control simulations for SO_2 (Figure 5) than was seen for O_3 or NO_2. In particular, the diurnal cycle is affected, with much higher values being seen in the test run results for the early hours of the morning. In winter, the observed pattern of the diurnal cycle is better represented in the test run but not so at other times of year. Neither the control or test simulations represent patterns of variation in SO_2 as well as those of the other pollutant gases. This is true with respect to the diurnal cycles but also more generally as indicated by the much lower values of the correlation coefficient in Table 4. The correlations are very similar between the two simulations. However, the positive biases in all seasons are greater for the test run than for the control run. There are particularly large relative differences in spring, where the bias is about 3 times that of the control, and summer, where it is about twice as large. In all seasons though, the absolute difference in the bias is well below 1 µg m^{-3} and the implications for air quality forecasting are minimal since on site concentrations shown by the frequency distribution reach a maximum of 22 µg m^{-3}, a small fraction of that which would signify a pollution event. (89 µg m^{-3} is required to have any effect on the DAQI index.)

Much of the difference introduced by the change in aerosol scheme is likely to be due to the change in the diurnal variation in emissions which varies between SNAP sectors in AQUM-GLOMAP. Differences in sulphur chemistry may also be having an effect. The chemistry of SO_2 and DMS is heavily parameterised in CLASSIC, so may be significantly different from the RAQ-Aero sulphur chemistry in UKCA which is integrated with the whole chemistry mechanism. This may also have implications for the comparison of sulphate aerosol (see Section 4.3). To better understand the impact of changes in the chemistry scheme, a set of experiments with similar emission profiles for SO_2 in AQUM-GLOMAP and AQUM-CLASSIC could be set up for a more like for like comparison.

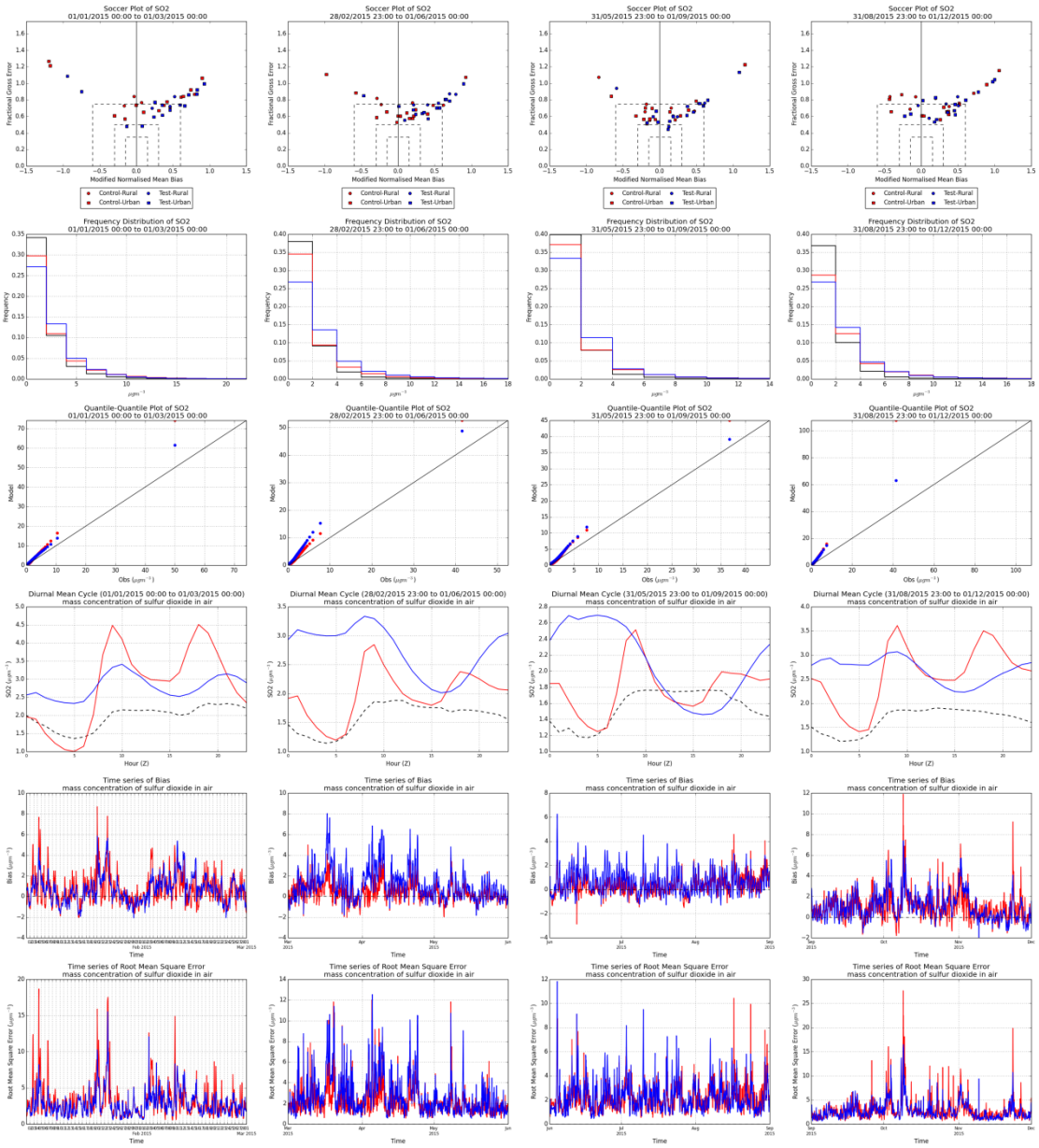

Figure 5. Statistical summaries of performance by meteorological season for SO_2, for the control run (red) and the test run (blue). Observational frequency distributions and mean diurnal cycles are included for reference (black). Seasons from left to right are winter (represented by January and February only), spring, summer and autumn.

Table 4. Seasonal performance metrics for SO_2

Statistic	Period	Control	Test
Correlation	JF	0.21	0.22
	MAM	0.28	0.26
	JJA	0.18	0.16
	SON	0.22	0.21
Bias (µg m^{-3})	JF	0.64	0.72
	MAM	0.38	1.17
	JJA	0.29	0.63
	SON	0.97	1.05
RMSE (µg m^{-3})	JF	3.90	3.22
	MAM	2.60	3.27
	JJA	2.43	2.60
	SON	3.68	3.26

4.2 Evaluation for Aerosol Pollutants

Figures 6 and 7 and Tables 5 and 6 show seasonal comparisons of the performance of test (AQUM-GLOMAP) and control (AQUM-CLASSIC) runs for $PM_{2.5}$ and PM_{10}. $PM_{2.5}$ and PM_{10} observations are represented by measurements at 44 and 32 AURN sites respectively. The most significant differences between the contributions to particulate matter between CLASSIC and the present GLOMAP-mode configuration are the absence of any nitrate contribution in GLOMAP and the absence of any sea-salt contribution over land in CLASSIC. To make the results for $PM_{2.5}$ and PM_{10} more comparable between the two aerosol schemes it is therefore useful to examine the results we would get with these components omitted from both schemes. These results are included in both figures and both tables accordingly. It should be noted that the adjusted PM for the control run still includes a small contribution from secondary organic aerosol which is absent from the test run, since monoterpene emissions are currently omitted. However, this contribution never reaches more than a few µg m^{-3}.

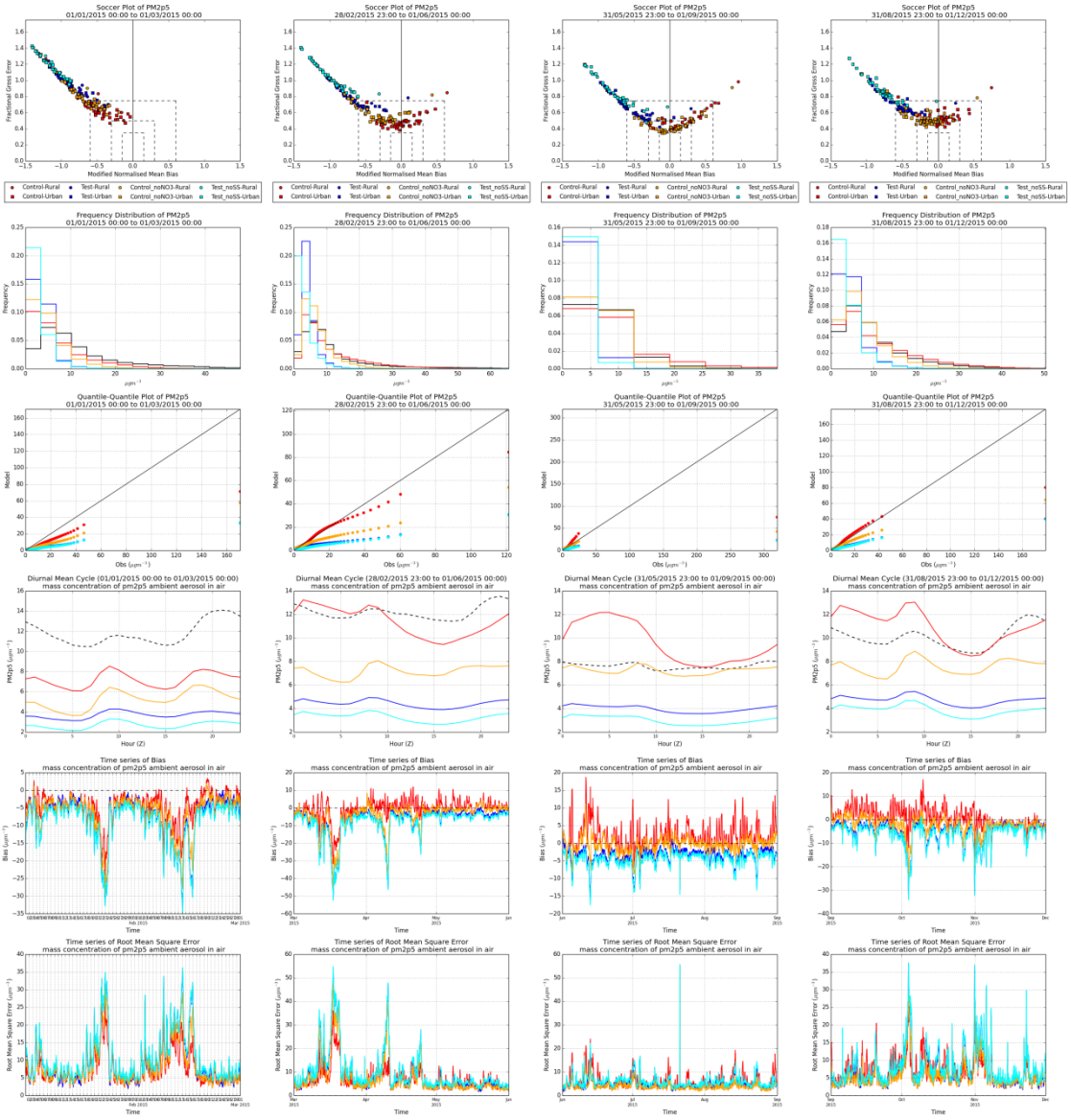

Figure 6. Statistical summaries of performance by meteorological season for $PM_{2.5}$, for the control run (red), the control run with the nitrate contribution subtracted (orange), the test run (blue) and the test run with the sea-salt contribution subtracted (cyan). The pair of adjusted runs (orange and cyan) provide the best like-for-like comparison between aerosol schemes. Observational frequency distributions and mean diurnal cycles are included for reference (black). Seasons from left to right are winter (represented by January and February only), spring, summer and autumn.

Table 5. Seasonal performance metrics for $PM_{2.5}$

Statistic	Period	Control		Test	
		$PM_{2.5}$	* $PM_{2.5}$ without NH_4NO_3	$PM_{2.5}$	* $PM_{2.5}$ without sea salt
Correlation	JF	0.67	0.61	0.50	0.59
	MAM	0.72	0.64	0.63	0.69
	JJA	0.53	0.46	0.45	0.48
	SON	0.62	0.61	0.60	0.62
Bias (µg m^{-3})	JF	-4.68	-6.64	-8.18	-9.20
	MAM	-0.62	-4.84	-7.60	-8.77
	JJA	1.84	-0.46	-3.63	-4.61
	SON	0.84	-2.54	-5.40	-6.26
RMSE (µg m^{-3})	JF	8.90	10.60	12.33	12.79
	MAM	8.45	10.87	13.12	13.62
	JJA	6.44	4.53	5.69	6.33
	SON	7.96	7.35	9.07	9.51

* These two columns provide the best like-for-like comparison between aerosol schemes

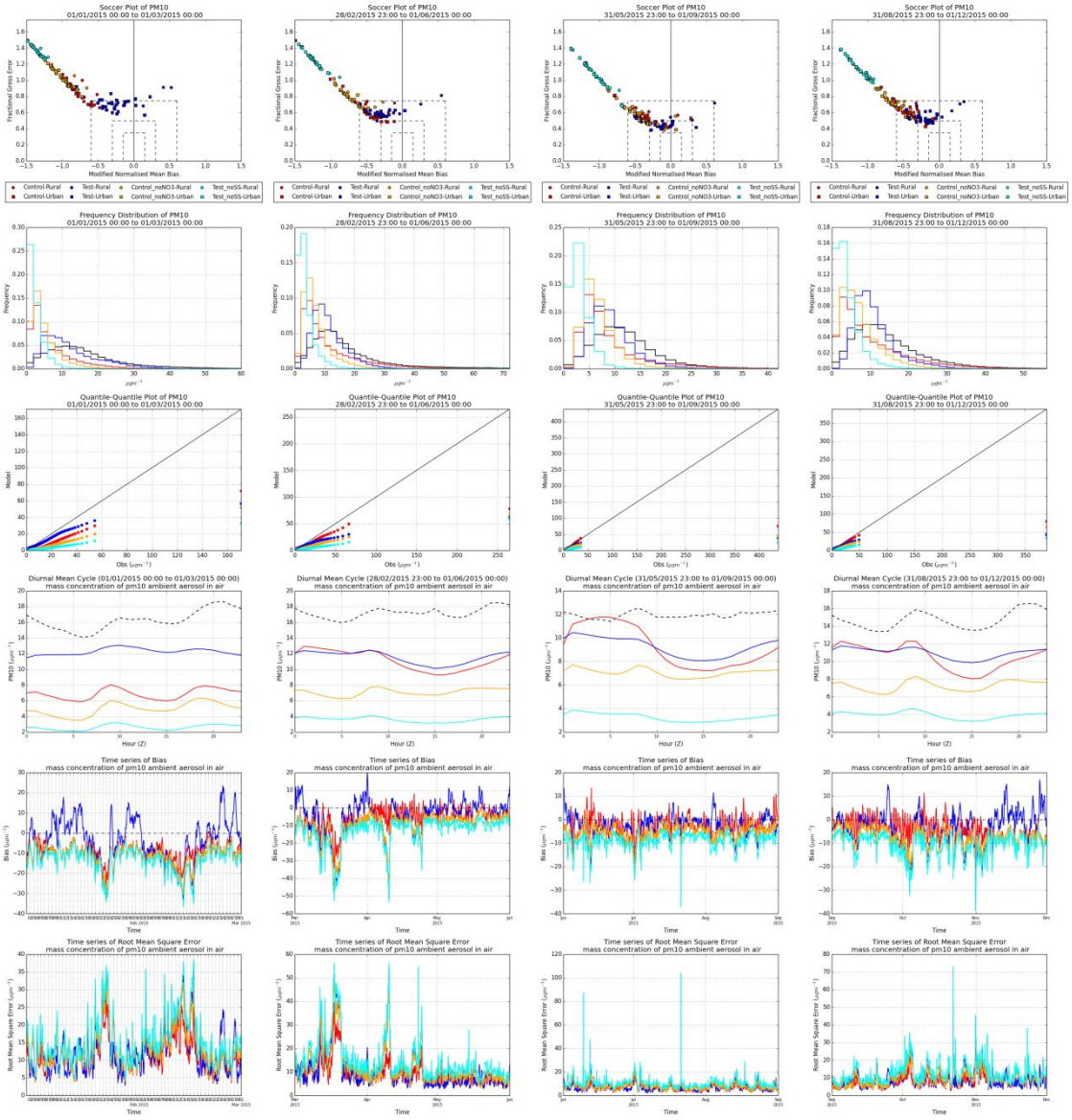

Figure 7. Statistical summaries of performance by meteorological season for PM_{10}, for the control run (red), the control run with the nitrate contribution subtracted (orange), the test run (blue) and the test run with the sea-salt contribution subtracted (cyan). The pair of adjusted runs (orange and cyan) provide the best like-for-like comparison between aerosol schemes. Observational frequency distributions and mean diurnal cycles are included for reference (black). Seasons from left to right are winter (represented by January and February only), spring, summer and autumn.

Table 6. Seasonal performance metrics for PM_{10}

Statistic	Period	Control		Test	
		PM_{10}	* PM_{10} without NH_4NO_3	PM_{10}	* PM_{10} without sea salt
Correlation	JF	0.61	0.58	-0.07	0.57
	MAM	0.69	0.60	0.09	0.58
	JJA	0.44	0.40	0.24	0.40
	SON	0.57	0.57	0.19	0.58
Bias (µg m^{-3})	JF	-9.37	-11.32	-3.98	-13.69
	MAM	-5.74	-9.88	-5.55	-13.38
	JJA	-3.09	-5.32	-2.89	-9.02
	SON	-4.33	-7.56	-3.80	-10.89
RMSE (µg m^{-3})	JF	12.95	14.78	14.64	17.01
	MAM	11.03	14.56	14.76	17.53
	JJA	8.26	8.62	8.12	11.34
	SON	9.90	11.19	11.09	13.86

* These two columns provide the best like-for-like comparison between aerosol schemes.

The effect of sea-salt on PM_{10} in GLOMAP is large, as seen from a quick inspection of Figure 7. A lesser effect is seen on $PM_{2.5}$ in Figure 6 because of the large mean diameter of the sea-salt particles. The impact of sea-salt can be widespread as shown by the snapshot shown in Figure 8. This is taken on 29th January, during a period in which the differences between the adjusted and unadjusted test run PM_{10} bias in Figure 7 is particularly pronounced. At this time, contributions to $PM_{2.5}$ in particular are similar over much of the country to those over the sea, demonstrating the importance of considering advective transport of the particles. Although a greater fraction of the larger particles are apparently lost (presumably as a result of deposition), the corresponding PM_{10} over many parts of the country is very high: over 20 µg m^{-3} throughout most of England and Wales and over 30 µg m^{-3} in some areas. Assuming for the moment that the transport in GLOMAP is reasonably realistic, these results suggest that the inclusion

of sea-salt advection may have the potential to improve predictive skill for PM at AURN sites significantly by introducing an important source of aerosol that is missing from CLASSIC.

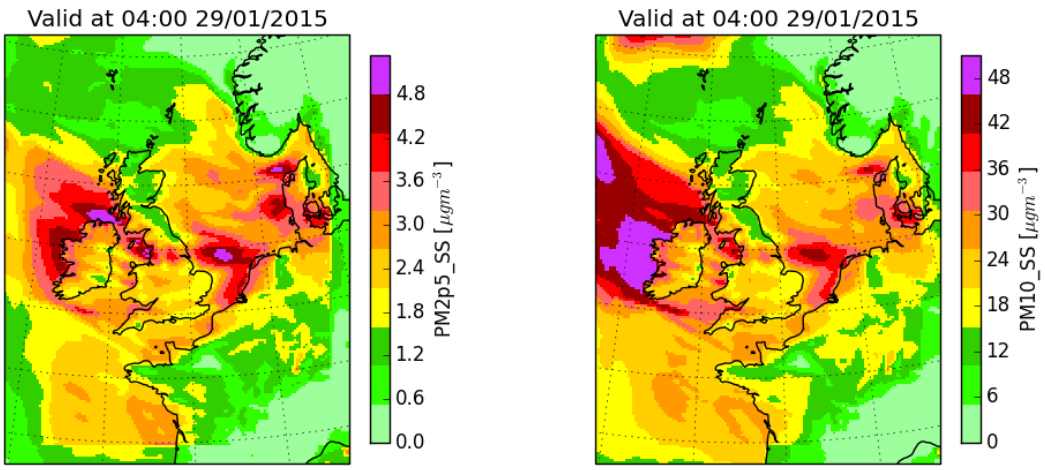

Figure 8. Contributions of sea-salt aerosol to $PM_{2.5}$ and PM_{10} in the AQUM-GLOMAP test simulation during a period of elevated sea-salt concentrations over land at the end of January 2015.

The most striking difference between the control and test simulations is the much lower levels of $PM_{2.5}$ in the GLOMAP test run in all seasons (Figure 6). From the bias statistics in Table 5, mean seasonal concentrations are lower in the test run by an amount between about 3.5 µg m^{-3} (winter) and about 7 µg m^{-3} (spring). These differences can in part be attributed to the absence of a nitrate scheme in GLOMAP but not wholly, since the concentrations are still greater for the adjusted CLASSIC control run with the nitrate concentration removed, despite the presence of a sea-salt contribution in GLOMAP. When adjustments are applied for both nitrate and sea-salt, the differences in seasonal mean concentrations are between about 2.6 µg m^{-3} (winter) and about 4.2 µg m^{-3} (summer). The suggestion is that even with a nitrate scheme the GLOMAP scheme would be expected to increase the size of the negative bias in winter and is likely to over-correct for the positive bias in summer (currently 1.84 µg m^{-3} in the control run), thereby introducing a negative bias in summer too. The reasons for the tendency

towards lower $PM_{2.5}$ in GLOMAP will be explored in more detail in Section 4.3 by comparing results for individual contributing aerosol species that are common to both schemes.

The correlation with observations is worse for all seasons in the test run than in the control. This is true even when the control run is adjusted by removing the nitrate contribution. However, the differences are then almost negligible with the exception of the winter-time results. The reduction shows that nitrate is a key factor in increasing the model's predictive skill for $PM_{2.5}$. Surprisingly, the correlation results for the test run actually improve when the sea-salt contribution is removed, although the RMS errors are slightly worse because of increased negative biases. This suggests that sea-salt concentrations in the current GLOMAP model configuration are in poor agreement with real-world concentrations.

The results for PM_{10}, for which sea-salt is a much larger contributor than $PM_{2.5}$, show a much more dramatic reduction in correlation coefficient for the GLOMAP test run with respect to the control. Yet the correlation results without the sea-salt contribution are very similar to the control without the nitrate contribution and only a little less when the nitrate contribution is included. The very low correlation coefficients for the unadjusted test run early in the year (0.09 in spring and actually negative in winter at -0.07) serve to underline the limitations of the current sea-salt predictions given by this configuration. Nevertheless, the negative PM_{10} bias is much smaller in the test run before the sea-salt contribution is removed than after (Table 6). Furthermore, the test run PM_{10} with sea-salt included seems to reproduce the observed frequency distribution better than either the test run without sea-salt or the control (Figure 7). Both of these apparent improvements are evident in all seasons. Further development and analysis of the sea-salt scheme is required in order to test whether the reduced PM_{10} bias merely arises from it adding a compensating bias into the system or whether it is capable of adding real skill to the UK forecasts of PM_{10} and $PM_{2.5}$.

If we compare the tabulated seasonal PM_{10} biases in the test run with those in the control, we find they are generally similar despite the absence of any nitrate contribution in GLOMAP. This is apparently due to the compensating effect of sea-salt on bias reduction. In winter, when the sea-salt contribution is particularly high in GLOMAP, and when we might expect it to be larger in reality, the PM_{10} biases are actually much smaller

than in the control run. Further examination suggests that inclusion of a nitrate scheme may reduce these biases further without the risk of over-correcting them to any great extent. This is inferred from a comparison between the biases in the unadjusted test run PM_{10} and the differences between the PM_{10} biases in the control run with and without nitrate. A comparison between the adjusted PM_{10} for the two runs shows that there are factors that reduce PM_{10} in the GLOMAP run other than just the absence of nitrate. However, the differences in the seasonal mean concentrations shown by the bias statistics in Table 6 are broadly consistent with those identified for $PM_{2.5}$, suggesting that these factors are primarily affecting the smaller particles.

In view of the rather contradictory results attributable to the presence of advected sea-salt aerosol in GLOMAP, it is helpful to examine time series of PM_{10} at some of the AURN sites. A sample is shown in Figure 9. The time series illustrate the fact that the correlation is generally poor between the test run PM_{10} and the observations. However, the characteristics of the variability seem to be reproduced better by the test run than by the control, suggesting that the AQUM-GLOMAP run could be capturing some of the statistical properties of the variability in sea-salt but not accurately reproducing spatial patterns at the resolution required to represent the observed variability at individual sites. (A more detailed analysis, aggregating sites might help to disentangle the effects of spatial and temporal variability.) It is interesting to note that at Narberth in Pembrokeshire, near to the Welsh coast, there is good evidence of local correlation between the GLOMAP PM_{10} results and the observations. This is seen especially at the shorter time scales, from days to weeks, if we ignore the period in mid-February where ammonium nitrate contributions are likely to be more significant.

The general low correlation coefficients for the GLOMAP PM_{10} may in part be a consequence of the fact that sea-salt is sometimes an important PM_{10} component and sometimes not. Poor representation of patchiness in the sea-salt distribution because of the relatively low model resolution (12 km) could be a factor. Some more detailed investigation would be required to resolve this issue. Other aspects of the model configuration that affect sea-salt distributions should also be examined. Useful sensitivity tests would include the use of alternative sea-salt emissions parameterisations that are present in the code and the removal of sea-salt from LBCs to evaluate the relative importance of domain import versus in-domain production. For regions where patterns of imported sea-salt aerosol are significant, the quality of the sea-salt representation in the

global model providing the LBCs could be as critical as that of the 12 km model. To understand the importance of sea salt in reality, use of speciated PM observations (of sea salt and other components) will be crucial. This should lead to better understanding of the reasons for model bias in both CLASSIC and GLOMAP and drive improved forecast skill.

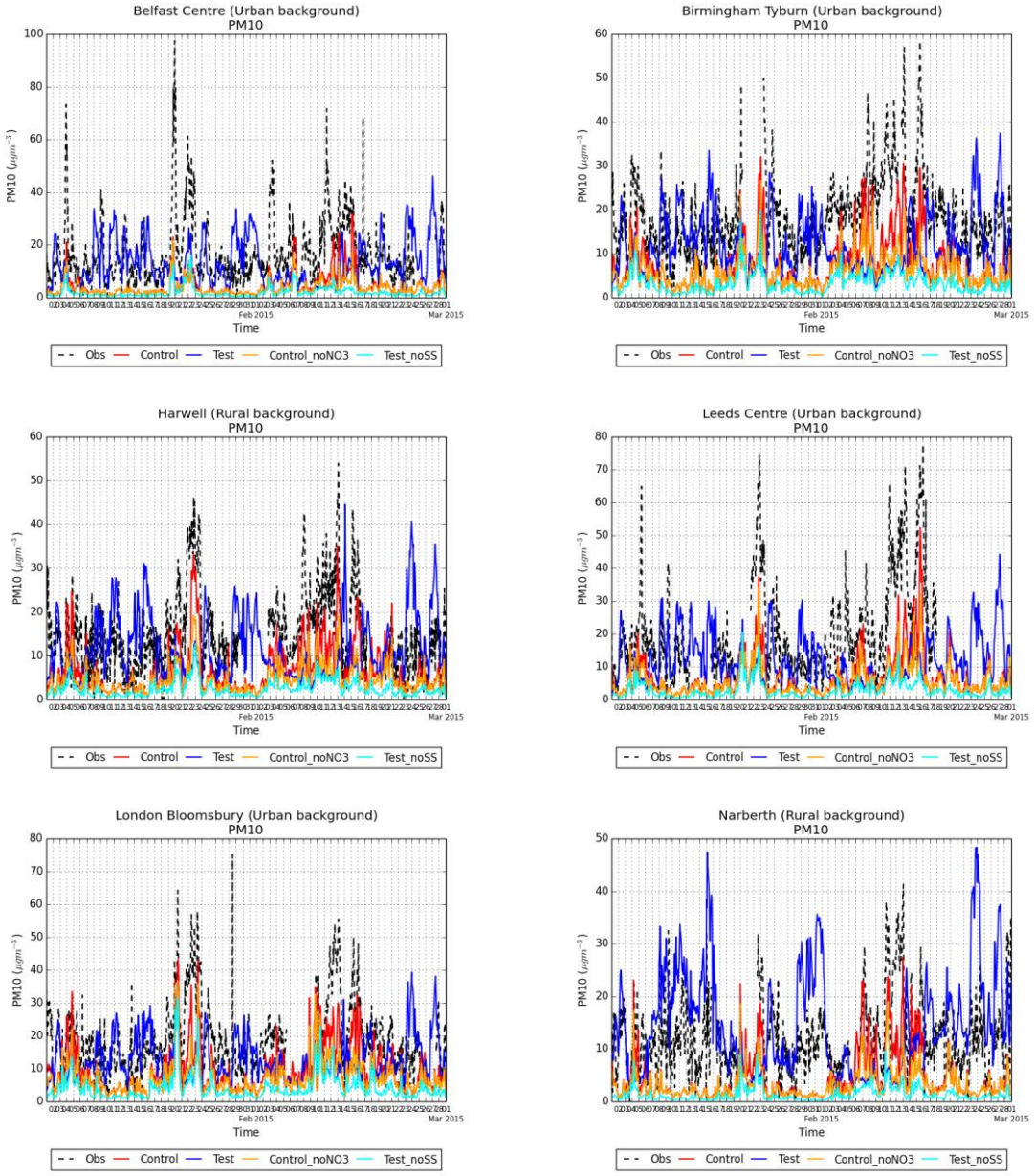

Figure 9. Model time series of PM_{10} at selected UK sites for the winter period (January and February). Trajectories are shown for the control run, the control run with the nitrate contribution subtracted, the test run and the test run with the sea-salt contribution subtracted. The observed PM_{10} is shown for reference.

4.3 Speciated PM Contributions

To examine the factors leading to reduced $PM_{2.5}$ in GLOMAP, other than the absence of a nitrate scheme, the speciated contributions to $PM_{2.5}$ from black carbon, organic carbon and sulphate are examined here. The comparison is complicated by the fact that a fraction of the total atmospheric concentration of both black and organic carbon in CLASSIC is represented as material from biomass burning. It is assumed in the CLASSIC aerosol scheme that 8.75% of fresh biomass and 5.4% of aged biomass is black carbon (and particle sizes for aged biomass are 20% larger so would contribute slightly less to PM). The ratio of fresh to aged biomass will vary in time and space but for simplicity we take an approximate mid-value of 7% of the total biomass $PM_{2.5}$ contribution to be black carbon and 93% to be organic carbon. The sulphate contribution in CLASSIC is in the form of ammonium sulphate while that in GLOMAP is from sulphuric acid. Units are converted to μg m^{-3} SO_4^{2-} for comparison purposes.

The seasonal frequency distribution and diurnal cycle comparisons in Figure 10 show that all components contribute consistently less to $PM_{2.5}$ throughout the year in the test run than in the control. Thus the tendency for GLOMAP to produce lower $PM_{2.5}$ concentrations is not attributable to differences in the representation of any one aerosol species. However, it is notable that the differences between test and control runs are much larger for the sulphate contribution than for the carbonaceous species. The diurnal cycles in Figure 10c show that seasonal mean contributions for sulphate are a factor of 6 or more lower in autumn and a factor of about 3 lower in spring and summer when the difference is least. This compares with typical reductions of about 1/3 for both black carbon and organic carbon. The lower sulphate concentrations are consistent with a slower oxidation of SO_2 in the GLOMAP configuration, which could also partly explain the higher concentrations of SO_2 noted in Section 4.1. More work to compare the chemistry schemes, including an examination of the fluxes of SO_2 to sulphate would be needed to confirm this.

a)

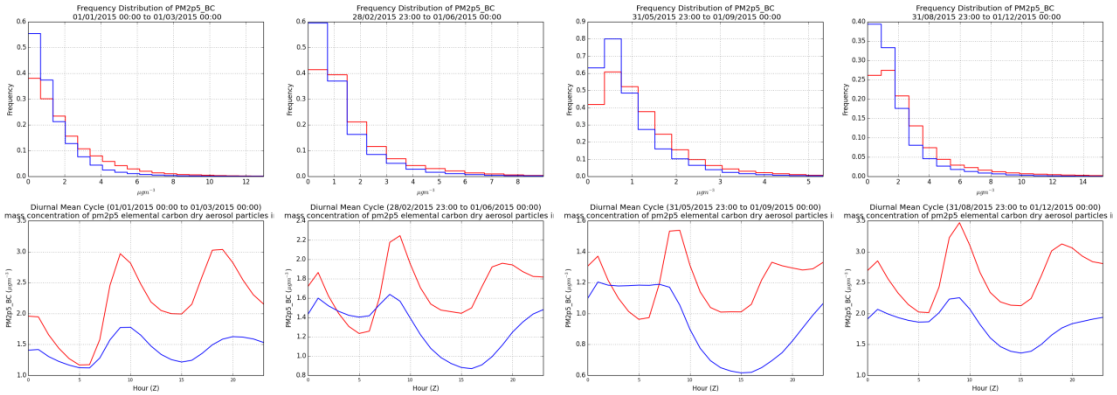

b)

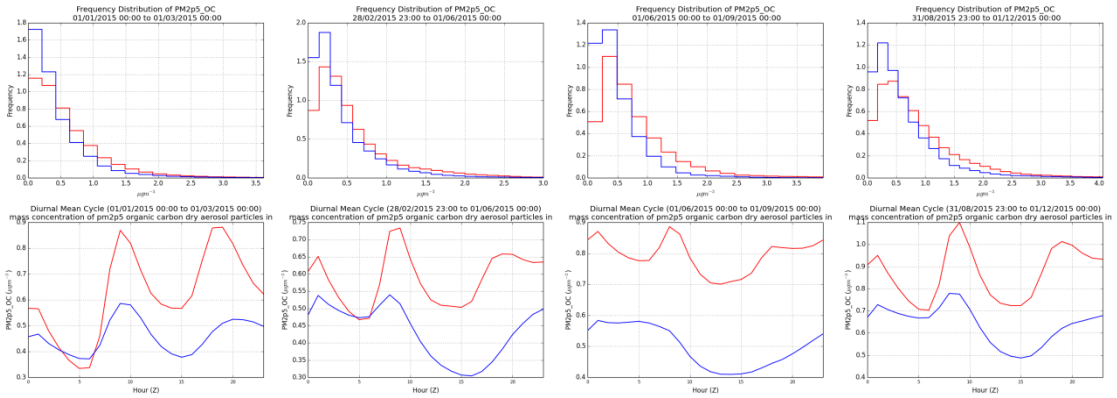

c)

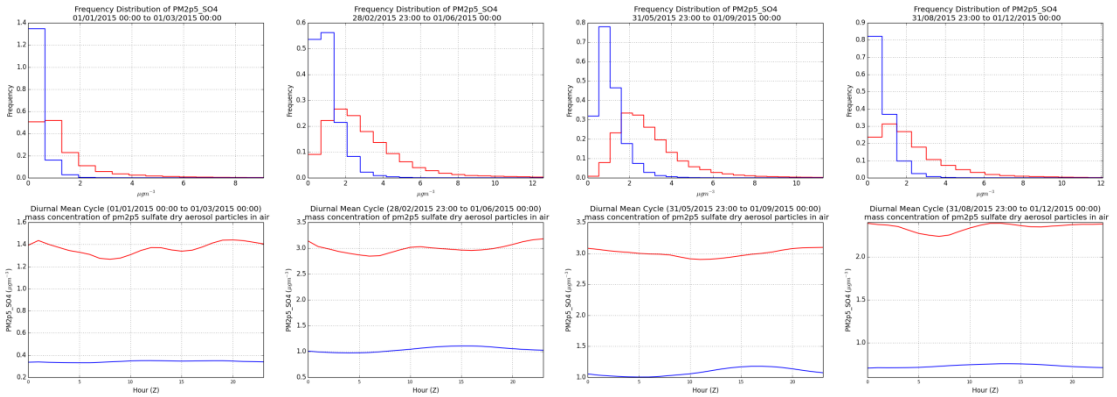

Figure 10. Frequency distributions and mean diurnal cycles by meteorological season for speciated $PM_{2.5}$, for the control run (red) and the test run (blue). (a) Black carbon contribution. (b) Organic carbon contribution. (c) Sulphate contribution. Seasons from left to right are winter (represented by January and February only), spring, summer and autumn.

Because of differences outlined in Section 2.3 in the way that PM is represented in the two schemes (apart from the difference in units which is corrected for), it is not immediately obvious to what extent differences in $PM_{2.5}$ between schemes reflect differences in the total mass of the contributing species present in the aerosol. Inspection of time series at AURN sites confirm that they do to a very large extent. Example time series of speciated $PM_{2.5}$ from the control and test runs shown alongside the total concentrations of the corresponding species in Figure 11 illustrate how the differences are primarily due to differences in total mass for all three species considered. In the case of the carbonaceous species, the total concentrations are almost identical to the corresponding $PM_{2.5}$ contributions because of the small particle sizes. (Small differences in peak values are an artefact introduced by the fact that tracer concentration fields were only output from the model at 3 hourly intervals, whereas the PM diagnostics are hourly.) For sulphate, the 2.5 µm cut-off makes a more significant difference. These time series from Harwell are typical of those from sites all over the UK.

a)

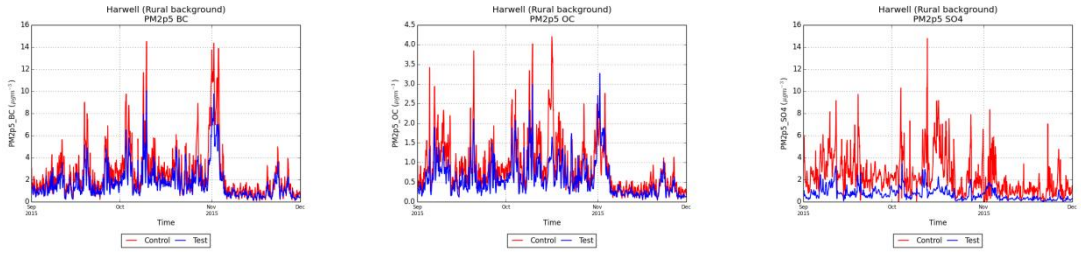

b)

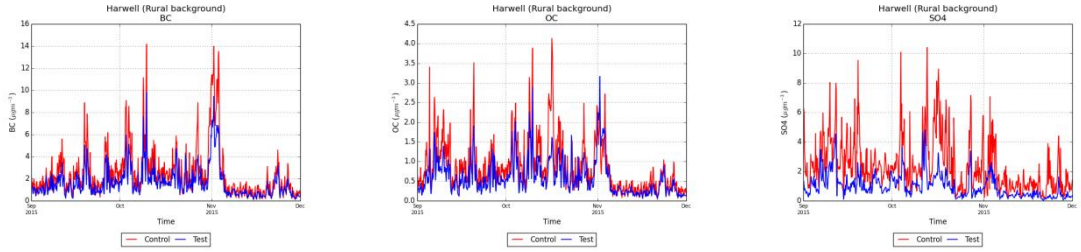

Figure 11. (a) Contributions to $PM_{2.5}$ from black carbon, organic carbon and sulphate at Harwell in the control and test runs over the autumn period. (b) Corresponding total mass concentrations for each aerosol component.

For sulphate, it is possible to investigate further by comparing the sulphate concentration in modes that are broadly comparable between the two schemes. Figure 12 shows comparisons for Harwell and once again the general patterns shown are typical of sites across the UK. For the purposes of the comparison, equivalence is assumed between (a) the CLASSIC sulphate Aitken mode and the sulphate component of the GLOMAP Aitken mode (b) the CLASSIC sulphate accumulation mode and sulphate in the GLOMAP accumulation mode and (c) the CLASSIC sulphate dissolved mode and sulphate in the GLOMAP coarse mode. This is reasonable considering the geometric mean diameters for the fixed log-normal modes in CLASSIC and the corresponding variable log-normal modes in GLOMAP: the Aitken and accumulation modes in CLASSIC are defined with geometric mean diameters of 0.013 µm and 0.19 µm. These are compatible with GLOMAP ranges for the geometric mean diameters for Aitken mode of 0.01-0.1 µm and for accumulation mode of 0.1-0.5 µm.

It is apparent from the Harwell time series that much more of the material ends up in the largest mode in the GLOMAP aerosol representation (coarse mode) than in CLASSIC (dissolved mode). This largest mode is associated with material in cloud water droplets and the material is susceptible to wet deposition losses due to rainout. It seems likely then that the much lower concentrations in GLOMAP are at least partly a consequence of more material being contained within larger particles. A similar analysis for the carbonaceous species is less straightforward because the modes used to represent these species are not directly comparable between the aerosol schemes but it is possible that particle size and its implication for deposition loss is a contributory factor to the reduced concentration for these species too.

a)

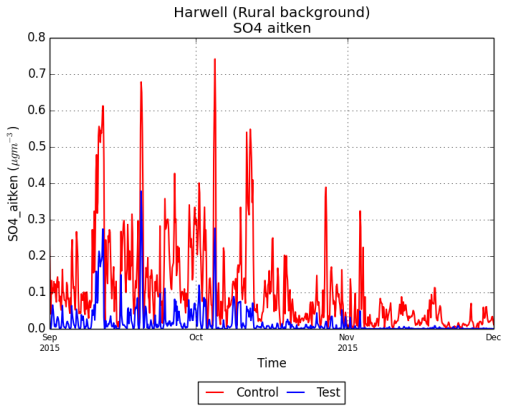

b)

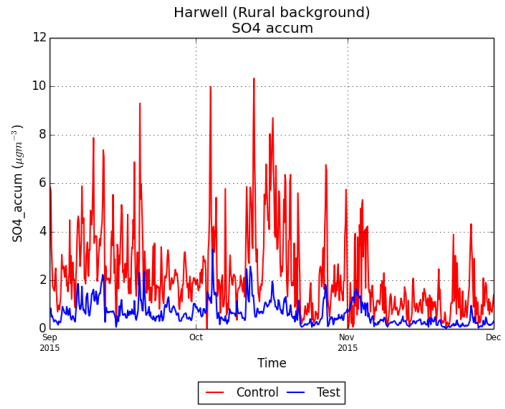

c)

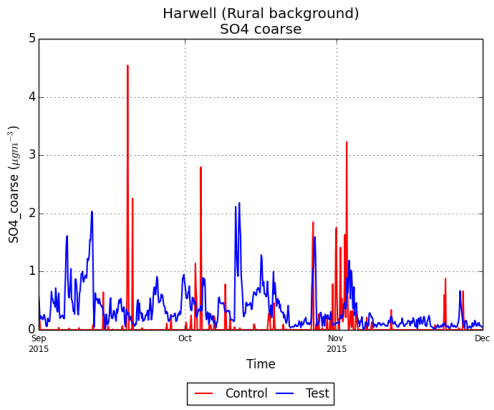

Figure 12. Division of sulphate between size modes that are directly comparable in the control and test runs. Time series over the autumn period at Harwell are shown for (a) the CLASSIC sulphate Aitken mode and the sulphate component of the GLOMAP soluble Aitken mode. (b) the CLASSIC sulphate accumulation mode and sulphate in the GLOMAP soluble accumulation mode and (c) the CLASSIC dissolved mode and sulphate in the GLOMAP soluble coarse mode.

As a final note regarding the aerosol composition, GLOMAP includes an explicit representation of water associated with each of the soluble aerosol modes. This makes it possible to diagnose the atmospheric concentration of PM at ambient conditions. It is interesting then to compare this concentration with the dry PM concentration that is intended to be consistent with the PM measurements, remembering that some fraction of the aerosol's water content, albeit a relatively small one, may not be removed in the measurement process as discussed in Section 2.3. Figure 13 shows such a comparison for Harwell.

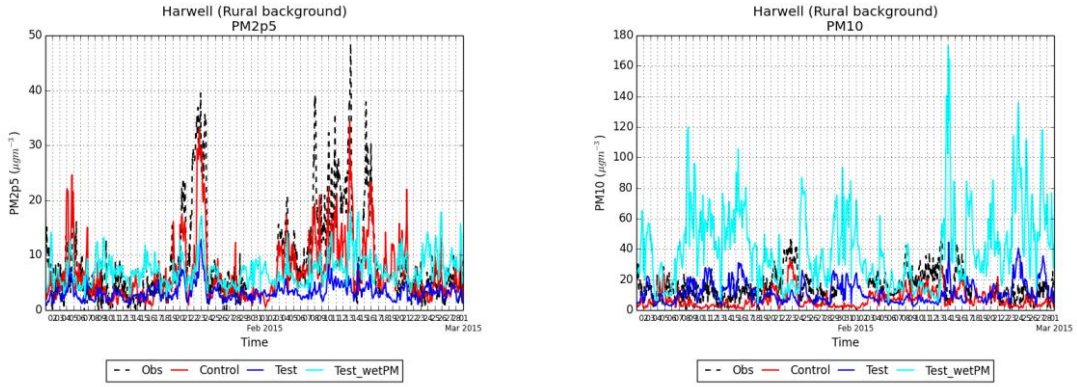

Figure 13. A comparison between the ambient and dry concentrations of $PM_{2.5}$ and PM_{10} diagnosed in the AQUM-GLOMAP test run (cyan and blue respectively). Concentrations from the AQUM-CLASSIC control run, based on dry PM, are shown for reference (red) together with measured PM (black). The time series are for the autumn period at Harwell.

The explicit representation of water associated with the aerosol in GLOMAP potentially opens the way to a more sophisticated treatment of factors affecting water content of PM at the standard measurement conditions. The wet PM concentration shown here can be interpreted as an upper limit for the modelled PM. It is not generally expected to be comparable with the observations because it is highly sensitive to ambient conditions, which may be wetter or sometimes drier than the measurement conditions. However, in

principle the equilibrium solution for water content could be re-calculated in the diagnosis of $PM_{2.5}$ and PM_{10} so that it is consistent with the measurements made at approximately 50% relative humidity. Such a modification of the simulated PM should reduce the tendency towards negative bias that we get from using dry PM concentration.

5. Summary and Conclusions

An initial evaluation of the GLOMAP-mode aerosol scheme as a possible replacement for the main elements of the CLASSIC scheme in the AQUM forecast system has been carried out. The replacement of the CLASSIC dust scheme is not considered. At this stage GLOMAP does not have a nitrate scheme suitable for operational use. In view of the dominance of ammonium nitrate aerosol in many UK pollution episodes, this is a major limitation and replacement of CLASSIC by GLOMAP for UK air quality modelling would not be considered until a suitable nitrate scheme was available. Here, GLOMAP is evaluated without any nitrate scheme so any evaluation can only be provisional.

The key findings are as follows.

- The performance of the model for O_3 and NO_2 is not significantly affected other than by the introduction of minor increases in concentration, attributable to the omission of heterogeneous chemistry on aerosol surfaces in the present AQUM-GLOMAP version.

- SO2 concentrations tend to be a little higher, leading to large relative increases in positive bias in spring and summer. However, concentrations remain far too small to affect the DAQI index so the implications for air quality forecasting are minimal.

- Mean seasonal $PM_{2.5}$ concentrations are reduced by an amount between about 3.5 µg m^{-3} (winter) and about 7 µg m^{-3} (spring), increasing the tendency towards negative bias in winter and spring and introducing negative biases in summer and autumn. Less than half of the reduction is likely to be attributable to the absence of a nitrate scheme in GLOMAP. The remainder could in part be attributed to a tendency towards increased particle sizes in the GLOMAP aerosol

and consequent increases in deposition losses. There is some evidence of this for sulphate, for which total aerosol concentrations are much reduced while concentrations in the largest size mode tend to be much higher.

- $PM_{2.5}$ concentrations are less well correlated with observations but results suggest that this effect is primarily attributable to the absence of a nitrate scheme.

- Negative biases in PM_{10} that occur in all seasons are reduced, especially in winter. This is attributable to the introduction of a prognostic sea-salt aerosol that more than compensates for any increased negative bias due to the absence of a nitrate contribution. The bias reduction still leaves scope for further reduction to be achieved with the introduction of a nitrate scheme.

- A detrimental effect is seen on the seasonal PM_{10} correlation statistics, particularly for winter when there is no evidence of any overall positive correlation with the observations. This detrimental effect is also attributable to the prognostic sea-salt aerosol and severely compromises any potential increase in predictive skill from its introduction. However, the introduction of sea-salt does improve the frequency distribution of PM_{10} and seems to better represent the characteristics of its temporal variability.

The effect of the prognostic sea-salt aerosol may prove to be beneficial overall. However, more investigation would be required to resolve the causes of its detrimental effect on the correlation statistics before operational use could be considered. Similarly, the greater tendency towards negative bias in $PM_{2.5}$ could prove to be a cause for some concern and may require further investigation. In both cases, a thorough investigation is difficult because of the missing nitrate scheme but useful work could be done to better understand the importance of LBCs for sea salt and to make use of speciated PM observations to evaluate and improve the predictions for the components currently modelled.

Another development which should be considered to help improve the PM bias is the inclusion of monoterpene emissions to produce biogenic SOA. The replacement of the 3-D SOA climatology used in CLASSIC by a prognostic scheme could potentially lead to

better representation of SOA during pollution episodes, although this is as yet untested. Anthropogenic SOA may also be of importance and should be considered for inclusion in AQUM-GLOMAP using the simple parameterisation described by Spracklen et al. (2011). For completeness, the climatological natural SO_2 emissions from volcanic activity that are used with CLASSIC in the current system should also be included, although these are of relatively low importance for the UK.

Another important consideration in any future evaluations of GLOMAP-mode for air quality modelling is the inclusion of feedback to the meteorology that is omitted in the present configuration. Full coupling between GLOMAP aerosols and meteorology should be considered, including both the direct effect of aerosols on radiation modelled by the UKCA RADAER scheme (Bellouin, 2010) and the indirect effects on cloud droplet formation and precipitation modelled by the UKCA Activate scheme based on the parameterisation of Abdul-Razzak and Ghan (2000).

The present study serves as a proof of concept, demonstrating that GLOMAP-mode has the potential to be an appropriate replacement for CLASSIC in the AQUM forecasting system, dependent on the future inclusion of a nitrate scheme suitable for operational use. Because GLOMAP is an aerosol scheme under active development and is much more sophisticated than CLASSIC, it has great potential to improve PM forecasts in the future but considerable effort will still be required even to get it to the point where it can replace CLASSIC for routine forecasting work. Some requirements for further analysis and development to realise that potential have been identified. A further consideration is the impact on computational resources, in particular the run-time for the UM forecast task which is a key factor in determining the time required to produce a 5 day air quality forecast operationally. The forecast task in the GLOMAP configuration of AQUM evaluated here has wall times that are typically 40-50% longer than those for the CLASSIC configuration. However, the present version does not benefit from improvements currently being made to enable greater optimization of the parallel features of the code and it should be possible to achieve significant reductions in the relative run-time with future UM versions.

Acknowledgements

This work relied heavily on the parallel activities of others in the Atmospheric Dispersion and Air Quality group developing and maintaining the AQUM forecasting system and on the support of the UM Systems team with key UKCA model developments. In particular, the authors would like to thank Stuart Whitehouse for implementation of the RAQ-Aero scheme in UKCA, Lucy Neal for support with adaptation of the AQUM emissions for GLOMAP-mode and Vivien Bright for help with the re-run archive of AQUM LBCs that was used in the evaluation experiments. Thanks are also due to Paul Agnew for advice throughout the evaluation project and to Graham Mann for helpful comments on the proposal document for the LBC conversion method.

References

Abdul-Razzak, H. and Ghan, S. J.: A parametrization of aerosol activation 2. Multiple aerosol types. Journal of Geophysical Research, 105(D5):6837–6844, 2000.

AQEG (Air Quality Expert Group): Fine Particulate Matter ($PM_{2.5}$) in the United Kingdom. Prepared for: Department for Environment, Food and Rural Affairs; Scottish Executive; Welsh Government; and Department of the Environment in Northern Ireland, 2012. Available at **https://www.gov.uk/government/publications/fine-particulate-matter-pm2-5-in-the-uk**

Bellouin. N.: Interaction of UKCA aerosols with radiation: UKCA RADAER. Technical report, Met Office, Exeter, 2010.

Bellouin, N., Rae, J, Jones, A., Johnson, C., Haywood, J. and Boucher, O.: Aerosol forcing in the Climate Model Intercomparison Project (CMIP5) simulations by HadGEM2-ES and the role of ammonium nitrate. J. Geophys. Res.-Atmos., 116, D20206, doi:10.1029/2011JD016074., 2011.

Cusack, S., Slingo, A., Edwards, J. M., and Wild, M.: The radiative impact of a simple aerosol climatology on the Hadley Centre atmospheric GCM. Q. J. Roy. Meteorol. Soc., 124, 2517–2526, 1998.

Liss, P. S., and Merlivat, L.: Air–sea gas exchange rates: Introduction and synthesis, in The Role of Air-Sea Exchange in Geochemical Cycling, edited by P. Buat-Ménard, pp. 113–127, Springer, New York, 1986.

Mann, G. W., Carslaw, K. S., Spracklen, D. V., Ridley, D. A., Manktelow, P. T., Chipperfield, M. P., Pickering, S. J. and Johnson, C. E.: Description and evaluation of GLOMAP-mode: a modal global aerosol microphysics model for the UKCA composition-climate model. Geosci. Model Dev., 3, 519-551, 2010.

Mann, G. W., Carslaw, K. S., Ridley, D. A., Spracklen, D. V., Pringle, K. J., Merikanto, J., Korhonen, H., Schwarz, J. P., Lee, L. A., Manktelow, P. T., Woodhouse, M. T., Schmidt, A., Breider, T. J., Emmerson, K. M., Reddington, C. L., Chipperfield, M. P. and Pickering, S. J.: Intercomparison of modal and sectional aerosol microphysics representations within the same 3-D global chemical transport model. Atmos. Chem. Phys., 12, 4449–4476, 2012.

Morgenstern, O., Braesicke, P., O'Connor, F. M., Bushell, A. C., Johnson, C. E., Osprey, S. M., and Pyle, J. A.: Evaluation of the new UKCA climate-composition model - Part 1: The stratosphere. Geosci. Model Dev., 2, 43–57, 2009.

O'Connor , F. M., Johnson, C. E., Morgenstern, O., Abraham, N. L., Braesicke, P., Dalvi, M., Folberth., G. A., Sanderson, M. G., Telford., P. J., Voulgarakis, A., Young, P. J., Zeng, G., Collins, W. I., and Pyle, J. A.: Evaluation of the new UKCA climate-composition model – Part 2: The troposphere, Geosci. Model Dev., 7, 41-91, 2014.

O' Dowd, C. D, Smith, M. H., Consterdine, I. E, and Lowe, J. A.: Marine aerosol, sea-salt, and the marine sulphur cycle: a short review. Atmos. Environ., 31, 73-80, 1997

Ordóñez, C., Savage, N. H., Agnew, P., and Neal, L. S.: Impact of the heterogeneous hydrolysis of N_2O_5 on pollutant concentrations in AQUM. Met Office, Exeter, 51pp, 2015.

Reddy, M. S., Boucher, O., Bellouin, N., Schulz, M.: Estimates of global multicomponent aerosol optical depth and direct radiative perturbation in the Laboratoire de Météorologie Dynamique general circulation model. J. Geophys. Res., 110, D10S16, 2005.

Rees, S. L., Robinson, A. L., Khlystov, A., Stanier, C. O., and Pandis, S. N.: Mass balance closure and the Federal Reference Method for $PM_{2.5}$ in Pittsburgh, Pennsylvania. Atmospheric Environment, 38, 3305-3318, 2004.

Savage, N. H., Agnew, P., Davis, L. S., Ordóñez, C., Thorpe, R., Johnson, C. E., O'Connor, F. M. And Dalvi, M.: Air quality modelling using the Met Office Unified Model (AQUM OS24-26): model description and initial evaluation. Geosci. Model Dev., 6, 353-372, 2013.

Spracklen, D. V., Jimenez, J. L., Carslaw, K. S., Worsnop, D. R., Evans, M. J., Mann, G. W., Zhang, Q., Canagaratna, M. R., Allan, J., Coe, H., McFiggans, G., Rap, A. and Forster, P.: Aerosol mass spectrometer constraint on the global secondary organic aerosol budget. Atmos. Chem. Phys., 11, 12109-12136, https://doi.org/10.5194/acp-11-12109-2011, 2011.

Wanninkhof, R.: Relationship between gas exchange and wind speed over the ocean, J. Geophys. Res., 97, 7373–7381, 1992.

Supplementary Material: Method for Conversion of C-IFS Aerosol Tracers to GLOMAP-mode Tracers in AQUM Lateral Boundary Conditions

May 2017

John Hemmings

An outline is given here of the proposed conversion of C-IFS model data to provide lateral boundary conditions for GLOMAP-mode MS2 (5 mode set-up) in the AQUM regional model. Section 1 describes the relevant C-IFS tracers. Section 2 describes the tracers required to represent the aerosol in GLOMAP-mode. Background information used in developing the conversion method is given in Sections 3 and 4. Section 5 then outlines the conversion procedure. An appendix is included with comparisons for test cases between C-IFS representation of the aerosol, based on assumed forms for particle size distribution, and the corresponding GLOMAP-mode representations obtained by applying the method,

1. C-IFS aerosol scheme tracers

The handling of aerosols in C-IFS is documented at https://atmosphere.copernicus.eu/documentation-global-products#Aerosols. C-IFS currently uses the IFS-LMD aerosol scheme which mainly follows the aerosol treatment in the LOA/LMD-Z model (Boucher et al. 2002; Reddy et al. 2005). There are 12 tracers.

- Dust, 3 bins (not required for GLOMAP-mode MS2, handled by CLASSIC)
- Sea-salt, 3 bins at 80% relative humidity
- Sulphate (SU)
- Hydrophobic organic matter (POM)
- Hydrophilic organic matter (POM)
- Hydrophobic black carbon (BC)
- Hydrophilic black carbon (BC)
- SO_2 (gas phase, no conversion required)

The tracers are mass mixing ratios for externally mixed aerosol components. The sea-salt bins have radius bounds at 0.03, 0.5, 5 and 20 microns. These were chosen so that roughly 10, 20 and 70% of aerosol mass was in each bin (Morcrette et al., 2009). For conversion to the aerosol representation of GLOMAP-mode MS2 (5 mode set-up), 8 C-IFS tracers must be considered. Dust is not represented in this set-up and will still be handled by CLASSIC. SO_2 is a gas phase tracer and does not contribute to the aerosol modes.

Wet sea-salt mass fluxes are integrated at 80% relative humidity so conversion to dry mass is required for GLOMAP-mode. To get back to dry matter, the documentation specifies a reduction factor of 4.3 for the mass mixing ratios and a reduction factor of 1.99 for the radii. These are consistent with conversion factors used by Morcrette at al. (2009) who assume a density of 2160 kg m^{-3} for dry particles and give a density for aerosol production at 80% RH of 1182 kg m^{-3}, based on the radius being twice that of the dry radius at this RH (Fitzgerald, 1975). This implies a conversion factor of 2160 / (1182 * 2^3) = 0.23

2. GLOMAP-mode tracers

- Nucleation mode (soluble): number, H2SO4, POM
- Aitken mode (soluble): number, H2SO4, BC, POM
- Accumulation mode (soluble): number, H2SO4, BC, POM, SS
- Coarse mode (soluble): number, H2SO4, BC, POM, SS
- Aitken mode (insoluble): number, BC, POM

Number tracers are particles per molecule of air (also referred to as number mixing ratio). H2SO4, BC, POM, SS are mass mixing ratios for the sulphuric acid, black carbon, particulate organic matter and sea-salt components in each internally mixed mode. The sulphuric acid tracer includes all of the sulphate aerosol that is represented. Particle size distributions for each mode are defined by variable mean diameter (dry), fixed geometric standard deviation and number ratio (total number of particles per molecule of air). Mode boundaries (for soluble modes) are defined with respect to particle geometric mean diameter. Standard deviations and boundaries are defined in Mann et al. 2010, with updates in Mann et al. 2012.

Geometric std. deviations: Nucleation = 1.59, Aitken(sol/ins) = 1.59, Accum. = 1.4, coarse = 2.0

Size ranges (geometric mean dry diameter): Nucleation = (< 10 nm), Aitken(sol/ins) = (10 – 100 nm), Accum. = (100 – 500 nm), Coarse = (> 500 nm)

3. Particle size distributions associated with C-IFS tracers

For inferring particle number concentrations and for distributing material between different modes we need information on the size distribution associated with each of the IFS aerosol mass mixing ratio tracers. Reddy et al (2005) assumed log-normal size distributions for the determination of optical properties in a global modelling study with the LMD model with parameters as specified in their Table 2. For sulphate, they used the size distribution of Boucher and Anderson (1995). That for BC (hydrophobic and hydrophilic) was from the Global Aerosol Data Set (GADS) (Köpke et al., 1997). For POM (hydrophobic and hydrophilic), they assumed the same size distribution as for sulphate. For sea-salt, for which the LMD model has a 10-bin representation, they used

a bi-modal distribution based on an analysis of a North Atlantic data set described by O'Dowd et al. (1997). In an analysis of optical properties for the C-IFS model, Morcrette et al. 2009 used the particle size distribution as simulated by the 3-bin scheme but also accounted for a fixed size distribution within each bin that had been calibrated against a model with more bins (presumably the LMD model).

For sulphate, BC and POM we will use the same size distributions as Reddy et al (2005). For sea-salt we will treat each bin separately as done by Morcrette at al. (2009). Within each bin, a uni-modal size distribution corresponding to the appropriate log-normal mode from O'Dowd et al. (1997) will be used. This is justified by an example in Section 3.2 below.

3.1 Reference distributions

Probability density functions (p.d.f.s) for each size distribution in terms of the particle radius r are given by

$$n(r) = \frac{1}{r \ln \sigma_g \sqrt{2\pi}} e^{-\frac{(\ln r - \ln \mu_g)^2}{2(\ln \sigma_g)^2}}$$

where μ_g and σ_g are the geometric mean and geometric standard deviation. This has unit area (by definition) and serves as a reference density function for number mixing ratio which can be scaled according to the total number mixing ratio (integrated over r) to get actual size distributions. Functions $n(r)$ for each C-IFS component are shown in Figure 1. The corresponding density function for mass mixing ratio is

$$m(r) = \frac{\rho N_A}{M_{air}} . \frac{4}{3} \pi r^3 n(r)$$

where ρ is the density of the particulate material, N_A is Avogadro's number and M_{air} is the molar mass of air. The function $m(r)$ will be referred to as the reference mass mixing ratio density function. Functions $m(r)$ for each C-IFS component are shown in Figure 2.

The values for μ_g , and σ_g and ρ are given in Table 1. The geometric mean is determined from the modal dry radius r_o by

$$\mu_g = e^{\ln r_o + (\ln \sigma_g)^2}.$$

Table 1. Parameters for C-IFS reference distributions				
	Modal dry radius (nm)	Geometric mean dry radius μ_g (nm)	Geometric std. deviation σ_g	Density of dry particles ρ (kg m^{-3})
Sulphate	35.5	57.4	2.0	1769
BC	11.8	19.0	2.0	1000
POM	35.5	57.4	2.0	1769
SS Bin 1	100	151	1.9	2160
SS Bin 2, SS Bin 3	1000	1617	2.0	2160

The tabulated size distribution parameters are those from Reddy et al. (2005) or for sea-salt, the equivalents for dry material. Note that some densities differ from GLOMAP-mode values. GLOMAP uses 1500 kg m^{-3} for BC and POM and 1600 kg m^{-3} for sea-salt. This difference will be automatically taken up by a shift in the GLOMAP-mode size distributions after conversion.

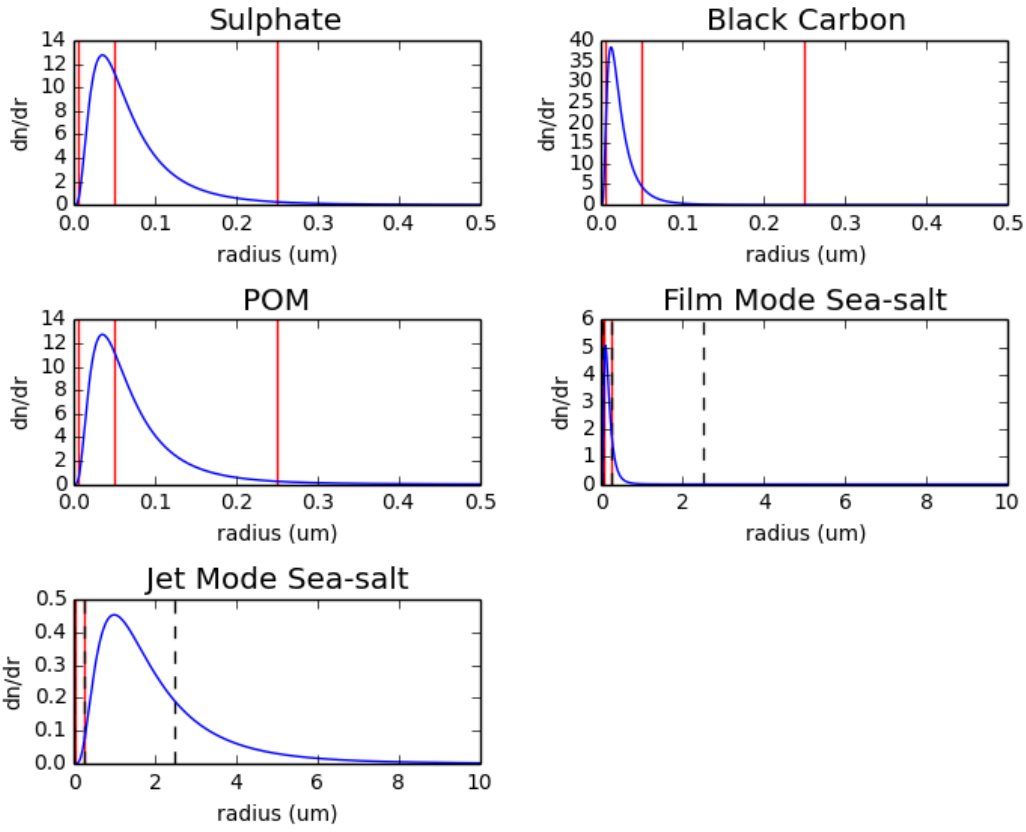

Figure 1. Number mixing ratio p.d.f.s (by dry radius) associated with C-IFS tracers. Black dotted lines show C-IFS bin boundaries. Red lines show GLOMAP mode boundaries. Film mode sea-salt is used for SS Bin 1 and Jet mode sea-salt for SS Bin 2 and SS Bin 3. Note that Sulphate and POM p.d.f.s are identical in the present implementation of the method.

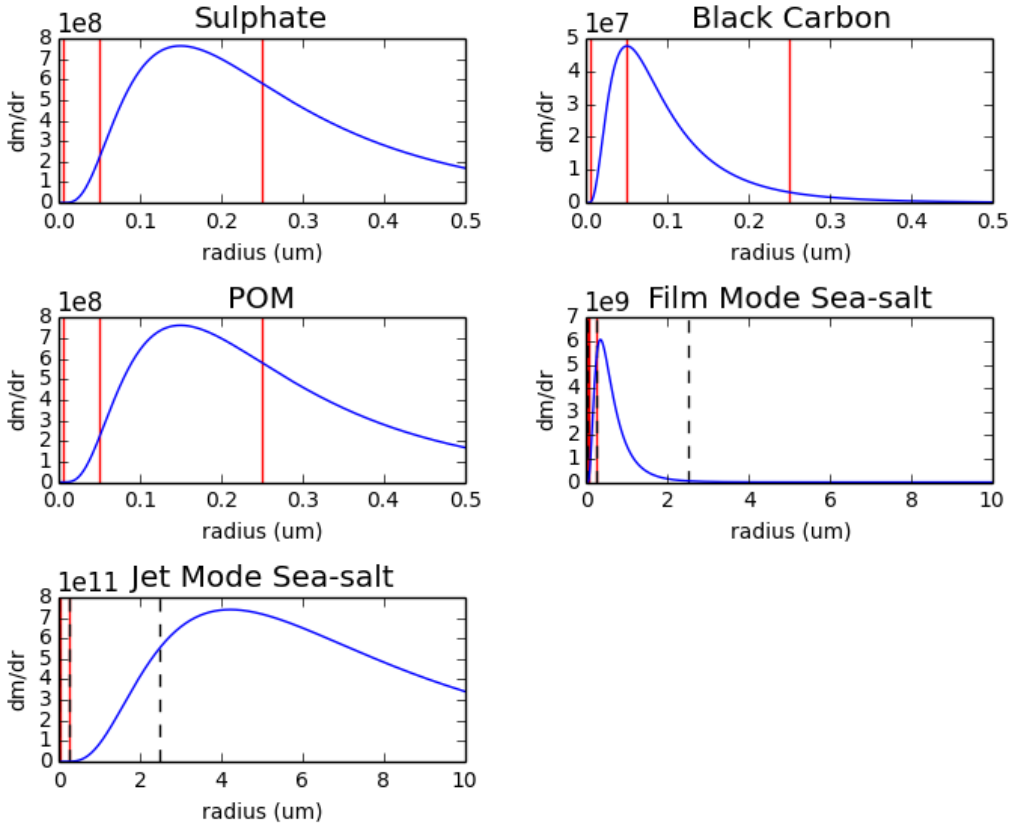

Figure 2. Reference mass mixing ratio density functions (by dry radius) associated with C-IFS tracers. Black dotted lines show C-IFS bin boundaries. Red lines show GLOMAP mode boundaries. Film mode sea-salt is used for SS Bin 1 and Jet mode sea-salt for SS Bin 2 and SS Bin 3. Note that Sulphate and POM density functions are identical in the present implementation of the method.

3.2 Identification of size distributions appropriate to C-IFS sea-salt bins

O'Dowd et al. (1997) present results from fitting a tri-modal distribution to sea-salt aerosol data with separate log-normal modes corresponding to film, jet and spume sources. Modal dry radii for material from each source were defined as 0.1, 1 and 6 µm for film, jet and spume respectively with corresponding geometric standard deviations of 1.9, 2 and 3. The following relations were obtained for total number concentration of particles (cm^{-3}) in each of the 3 modes as a function of 10 m wind speed ($m\ s^{-1}$):

$$\log_{10} N_{film} = 0.095\ U_{10} + 0.283$$

$$\log_{10} N_{jet} = 0.0422\ U_{10} - 0.288$$

$$\log_{10} N_{spume} = 0.069\ U_{10} - 5.81$$

These relations can be used to calculate the mass contribution of each mode to each of the C-IFS sea-salt bins by integrating the mass mixing ratio distributions $N_{film}\ m(r)$, N_{jet}

$m(r)$, $N_{spume}\ m(r)$ over each bin. Calculations were performed for wind speeds of 6, 9 and 17 m s^{-1}. The dominant contribution to SS Bin 1 (0.015 < r < 0.25 µm) was from Film mode with 99.8%, 99.9% and 99.96% of material for the 3 wind speeds. The dominant contribution to SS Bin 2 (0.25 < r < 2.5 µm) was from Jet mode with 94.8%, 92.7% and 82.8% of material for the 3 wind speeds. For SS Bin 3 (2.5 < r < 10 µm), the dominant contribution was also from Jet mode with 99.99%, 99.99% and 99.98% of material for the 3 wind speeds. (Note that bin ranges are given for dry radii.) Spume mode contributed less than 0.005% of material in all cases.

On this basis, the Film mode size distribution is used for SS Bin 1 and the Jet mode distribution for SS Bin 2 and SS Bin 3.

4. Soluble and insoluble modes

The two models handle the ageing of carbonaceous material differently, with potential implications for the division of material between soluble and insoluble modes.

In the IFS model, 50% of POM and 20% of BC are hydrophilic on emission. The fraction of hydrophilic material increases by transformation of hydrophobic POM or OC at a rate of 1.16 d^{-1} (Morcrette et al. 2009).

In GLOMAP-mode, all BC and POM aerosol emissions go into the insoluble Aitken mode. As a result of ageing, particles are transferred initially to the soluble Aitken mode (and can be transferred subsequently to other modes as a result of mode-merging). Ageing is associated with a mass flux from condensation of H_2SO_4 and SEC_ORG and accommodation of soluble material through inter-modal coagulation (Mann et al. 2010). No mass is transferred from the insoluble mode, only particle number.

The difference between the models in partitioning of emitted material between soluble and insoluble forms, in particular the large fraction of POM that is hydrophilic (soluble) in C-IFS, is offset by the fact that formation of soluble aerosol by nucleation of organic matter is not explicitly represented in C-IFS. A simple approach of transferring the hydrophilic material into soluble modes (including the nucleation mode for POM) and the hydrophobic material into the insoluble Aitken mode seems defensible as an initial approach.

Note that no distinction is made by Reddy at al. (2005) between the size distributions for hydrophilic and hydrophobic BC or for those for hydrophilic and hydrophobic POM. This contrasts with the situation in GLOMAP-mode where the soluble material is distributed over 3 modes (for BC) or 4 modes (for POM) while the insoluble material is represented by a single mode. Replacement of the Reddy et al (2005) carbonaceous aerosol distributions for with separate distributions for hydrophilic and hydrophobic material might therefore be beneficial in future.

5. Method for deriving GLOMAP-mode tracers

The LBC conversion scheme should conserve the mass of each component. Ideally, it should also conserve the particle number as defined by the assumed form of the C-IFS particle size distribution for each component.

Pre-calculated conversion factors will be used to convert from the C-IFS mass mixing ratios to number mixing ratios which define the corresponding size distributions. Then, for the soluble tracers (including hydrophilic BC and POM), further pre-calculated conversion factors will be used to partition number and mass between the GLOMAP modes according to the mode boundaries specified in terms of mean geometric radii.

For all modes (soluble and insoluble), the mean geometric radii implied by the initial allocation of material will be checked and adjustments to number concentration made if necessary to ensure that these radii are in the expected range. Where adjustments are necessary, number conservation is violated. This is acceptable since it is only mass that is defined explicitly by the C-IFS model and mass conservation is assured.

The steps are as follows.

1) Convert sea-salt at 80% relative humidity to dry mass.

2) For each C-IFS tracer, calculate number mixing ratio. Conversion factors from mass mixing ratio are given by a^{-1} where

$$a = \int_{r_0}^{r_1} m(r)dr$$

r_0 and r_1 being the lower and upper bounds of the bin (zero to infinity for un-binned tracers).

3) For each non-hydrophobic C-IFS tracer, partition number mixing ratio between the GLOMAP modes to which the material contributes. Conversion factors from number mixing ratio to partial number mixing ratio in a particular mode are given by

$$b_{\text{glomap}} = \int_{\max(r_0,\, r_{0\_\text{mode}})}^{\min(r_1,\, r_{1\_\text{mode}})} n(r)dr$$

where r_{0_mode} and r_{1_mode} are the mode boundaries, except that the lower bound for Aitken mode is set to zero in the case of black carbon and the lower bound for accumulation mode is set to zero in the case of sea-salt. This is because black carbon and sea-salt do not contribute to the smaller modes and any material that would otherwise end up in an invalid mode must be assigned instead to the smallest available mode. For hydrophobic tracers, the total number mixing ratio is assigned to the insoluble Aitken mode.

4) For each GLOMAP mode, sum partial number mixing ratio over all contributing components.

5) For each non-hydrophobic C-IFS tracer, partition mass mixing ratio between GLOMAP modes. Conversion factors from number mixing ratio to partial mass mixing ratio in a particular mode are given by

$$a_{\text{glomap}} = \int_{\max(r_0,\, r_{0\_\text{mode}})}^{\min(r_1,\, r_{1\_\text{mode}})} m(r)dr$$

Modified mode boundaries are used for black carbon and sea-salt as in Step 3. For hydrophobic tracers, the total mass mixing ratio is assigned to the insoluble Aitken mode.

6) For each GLOMAP mode containing SS, sum partial mass mixing ratio over SS contributions from each C-IFS bin. For the soluble modes, convert mass mixing ratio of sulphate to the equivalent mass mixing ratio of H_2SO_4.

7) For each GLOMAP mode, calculate geometric mean radius and if it is outside the expected range, determine a new number mixing ratio such that the new geometric mean radius is equal to the nearer of the mode boundaries. The geometric mean radius is given by

$$\mu_{\text{g}} = 0.5 \left(\frac{6\,V}{\pi \exp(4.5 \ln^2 \sigma_{\text{g}})}\right)^{\frac{1}{3}}$$

where

$$V = \frac{M_{\text{air}}}{N_{\text{A}}\, n_{\text{tot}}} \sum_{i=1}^{n_{\text{cpt}}} \frac{m_{\text{tot},i}}{\rho_i}$$

Here, n_{cpt} is the number of components contributing to the mode, n_{tot} is the number mixing ratio integrated over the mode's size distribution and $m_{\text{tot},i}$ is the corresponding mass mixing ratio for component i. These equations are consistent with Equations 5 and 6 in Mann et al. (2010). The new number mixing ratio is then given by solving the above for n_{tot}, given the required value for μ_{g} .

Conversion factors used in Steps 2, 3 and 5 are given in Table 2.

Table 2a. Factors for conversion from C-IFS m.m.r. to n.m.r. (a^{-1})
Also tabulated are factors for converting from total n.m.r. to n.m.r. in C-IFS bins (b) and from total n.m.r. back to m.m.r. in C-IFS bins (a)

	a^{-1}	b	a
Sulphate, POM	3.95e-09	1	2.53e+08
Black Carbon	1.9e-07	1	5.25e+06
Sea-salt Bin 1	1.9e-09	0.784	5.26e+08
Sea-salt Bin 2	1.97e-12	0.732	5.07e+11
Sea-salt Bin 3	2.28e-13	0.26	4.39e+12

Table 2b. Factors for conversion from C-IFS n.m.r. to GLOMAP n.m.r. by mode (b_{glomap})
(also shown as percentages with respect to totals given by b in Table 2a)

	nucl	Aitken	accum	coarse
Sulphate, POM	0.000215	0.421	0.562	0.0169
	0.0215%	*42.1%*	*56.2%*	*1.69%*
Black Carbon	0	0.918	0.0822	0.000103
	-	*91.8%*	*8.22%*	*0.0103%*
Sea-salt Bin 1	0	0	0.784	0
	-	-	*100%*	-
Sea-salt Bin 2	0	0	0	0.732
	-	-	-	*100%*
Sea-salt Bin 3	0	0	0	0.26
	-	-	-	*100%*

Table 2c. Factors for conversion from C-IFS m.m.r. to GLOMAP n.m.r. by mode (a_{glomap})
(also shown as percentages with respect to totals given by a in Table 2a)

	nucl	Aitken	accum	coarse
Sulphate, POM	2.71	2.87e+06	1.28e+08	1.22e+08
	1.07e-06%	*1.13%*	*50.6%*	*48.3%*
Black Carbon	0	1.29e+06	3.7e+06	2.7e+05
	-	*24.5%*	*70.3%*	*5.13%*
Sea-salt Bin 1	0	0	5.26e+08	0
	-	-	*100%*	-
Sea-salt Bin 2	0	0	0	5.07e+11
	-	-	-	*100%*
Sea-salt Bin 3	0	0	0	4.39e+12
	-	-	-	*100%*

Appendix: Comparing C-IFS and GLOMAP representations

Figures 3-4 show comparisons between C-IFS and GLOMAP-mode representations for a number of C-IFS test records. Number mixing ratio is shown together with mass mixing ratio for each type of material represented in both models (with C-IFS hydrophilic material equated to soluble material in GLOMAP and C-IFS hydrophobic material equated to insoluble material). Number and mass densities with respect to the log of the dry radius are plotted on a log-log scale to show relative differences in different parts of the size range. The C-IFS number and mass mixing ratio distributions are obtained from the C-IFS mass mixing ratios using the assumed size distributions described in Section 3. The GLOMAP distributions are those given by the sum of the contributing GLOMAP-modes corresponding to the GLOMAP tracer record obtained by application of the method described in Section 5.

Figure 3 (a-f) shows results for records with one type of material only having non-zero mass mixing ratio. Figure 4 (a-g) shows results for more realistic records in which there is interaction between components in the derivation of the GLOMAP representation. Note in particular that the primary cause of number mixing ratio non-conservation is the incompatibility between the size distribution assumed for the hydrophobic POM in C-IFS and the size range for the Aitken mode in GLOMAP.

Figure 4a is considered as a baseline case and the remaining figures show records derived from the baseline record as follows. Low SS: sea-salt reduced by 2 orders of magnitude; High SS: sea-salt increased by 2 orders of magnitude; Low BC: black carbon reduced by 2 orders of magnitude; High BC: black carbon increased by 2 orders of magnitude; Low Hydrophobic: hydrophobic material decreased by 2 orders of magnitude; High Hydrophobic: hydrophobic material increased by 2 orders of magnitude.

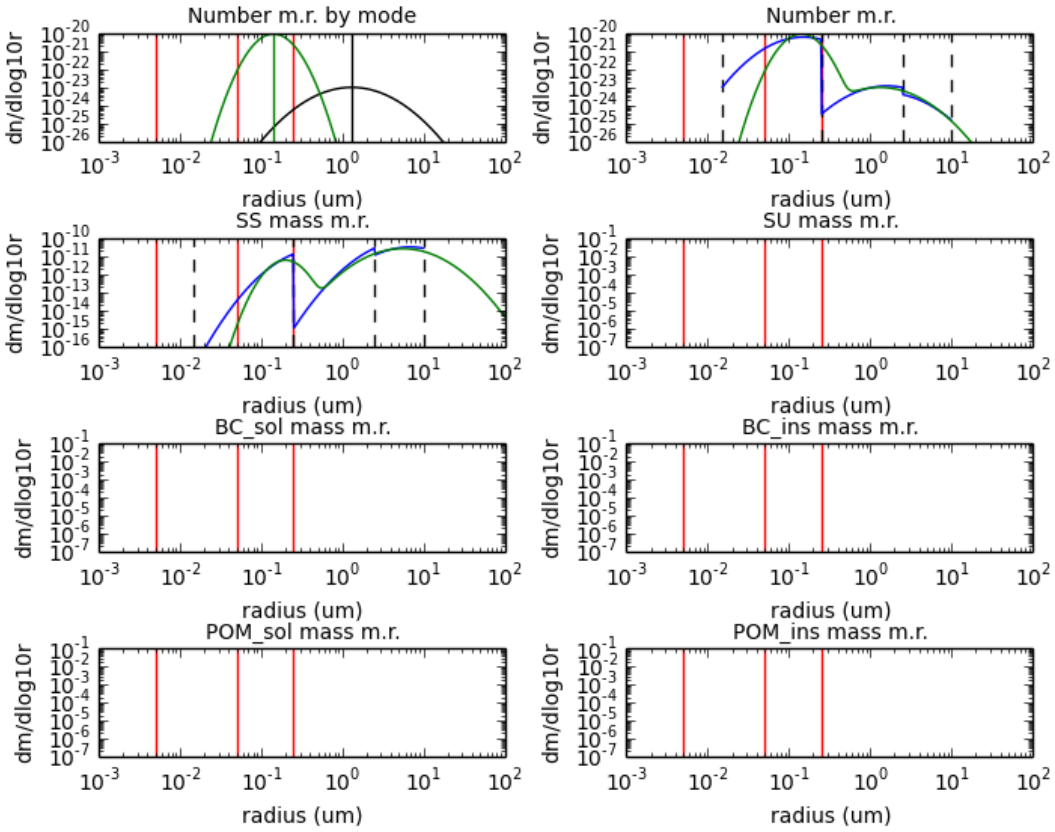

Figure 3a. C-IFS distributions (blue) and the corresponding GLOMAP-mode distributions (green) for **'SS only'** C-IFS test record. Black dotted lines show C-IFS bin boundaries. Red lines show GLOMAP mode boundaries. Top left: Number distributions for individual GLOMAP modes (blue = Nucleation Mode, cyan = Aitken Mode, green = Accumulation Mode, black = Coarse Mode; dotted line indicates the insoluble Aitken mode). The geometric mean radius for each mode is shown by a vertical line.

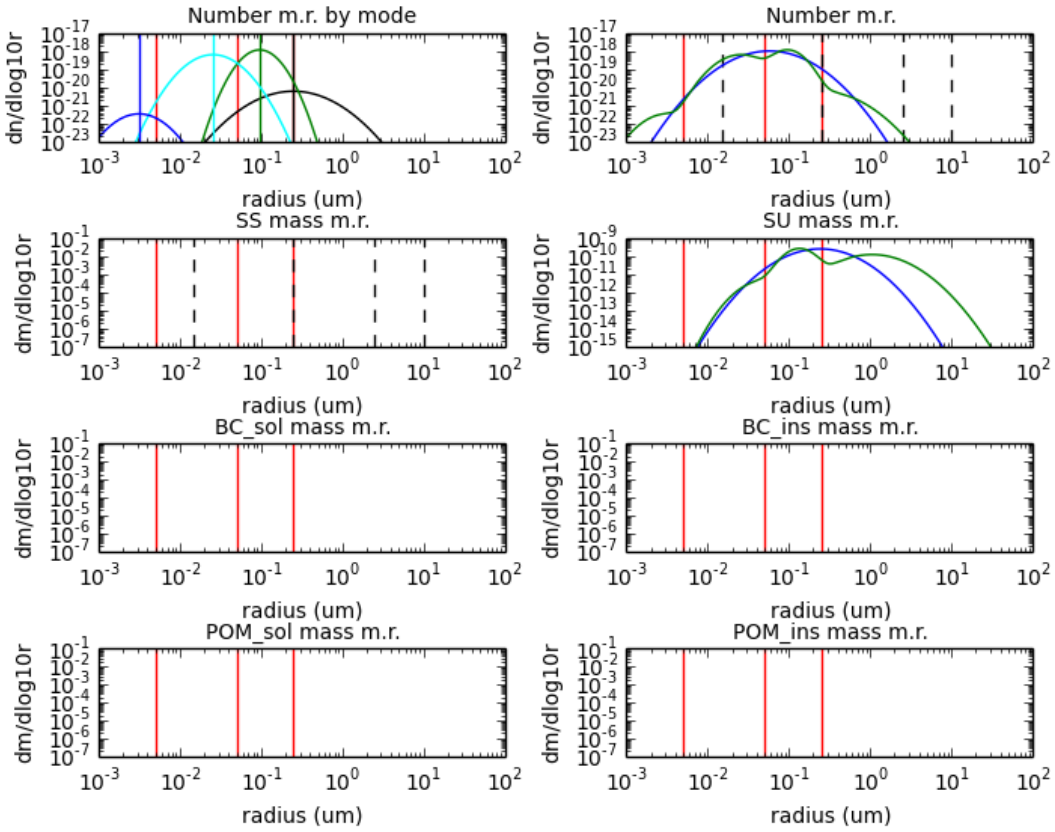

Figure 3b. C-IFS distributions (blue) and the corresponding GLOMAP-mode distributions (green) for **'Sulphate only'** C-IFS test record. Black dotted lines show C-IFS bin boundaries. Red lines show GLOMAP mode boundaries. Top left: Number distributions for individual GLOMAP modes (blue = Nucleation Mode, cyan = Aitken Mode, green = Accumulation Mode, black = Coarse Mode; dotted line indicates the insoluble Aitken mode). The geometric mean radius for each mode is shown by a vertical line.

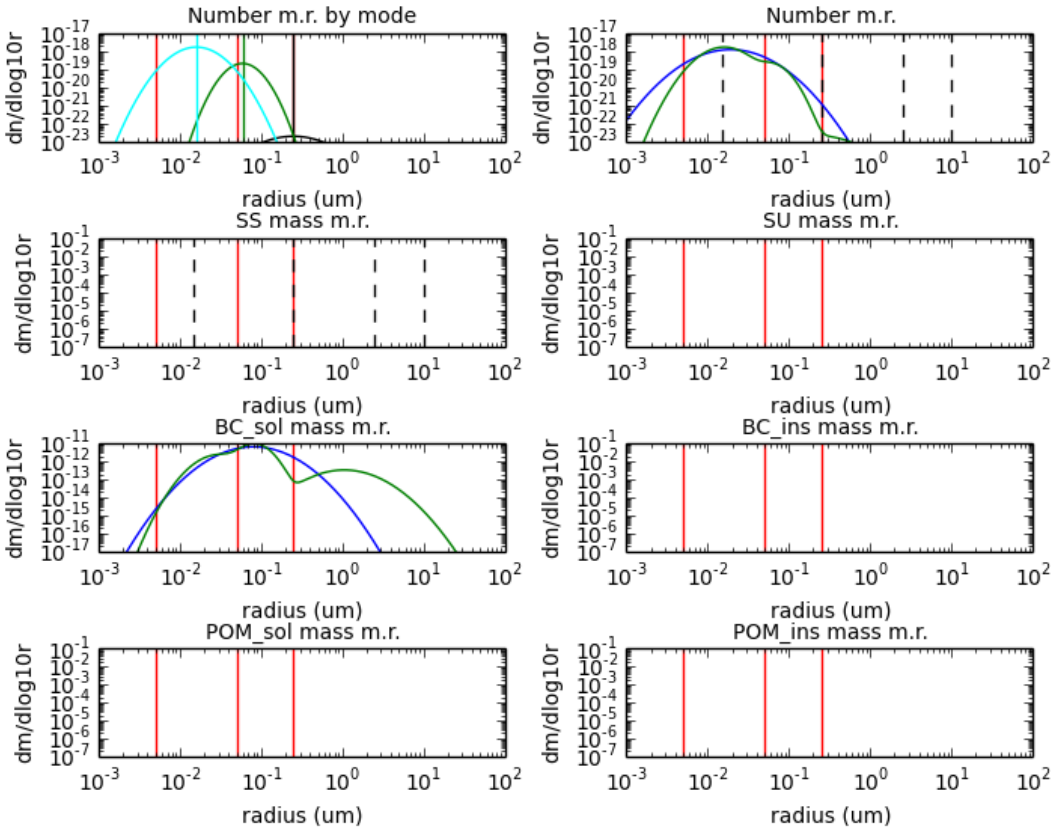

Figure 3c. C-IFS distributions (blue) and the corresponding GLOMAP-mode distributions (green) for **'Hydrophilic BC only'** C-IFS test record. Black dotted lines show C-IFS bin boundaries. Red lines show GLOMAP mode boundaries. Top left: Number distributions for individual GLOMAP modes (blue = Nucleation Mode, cyan = Aitken Mode, green = Accumulation Mode, black = Coarse Mode; dotted line indicates the insoluble Aitken mode). The geometric mean radius for each mode is shown by a vertical line.

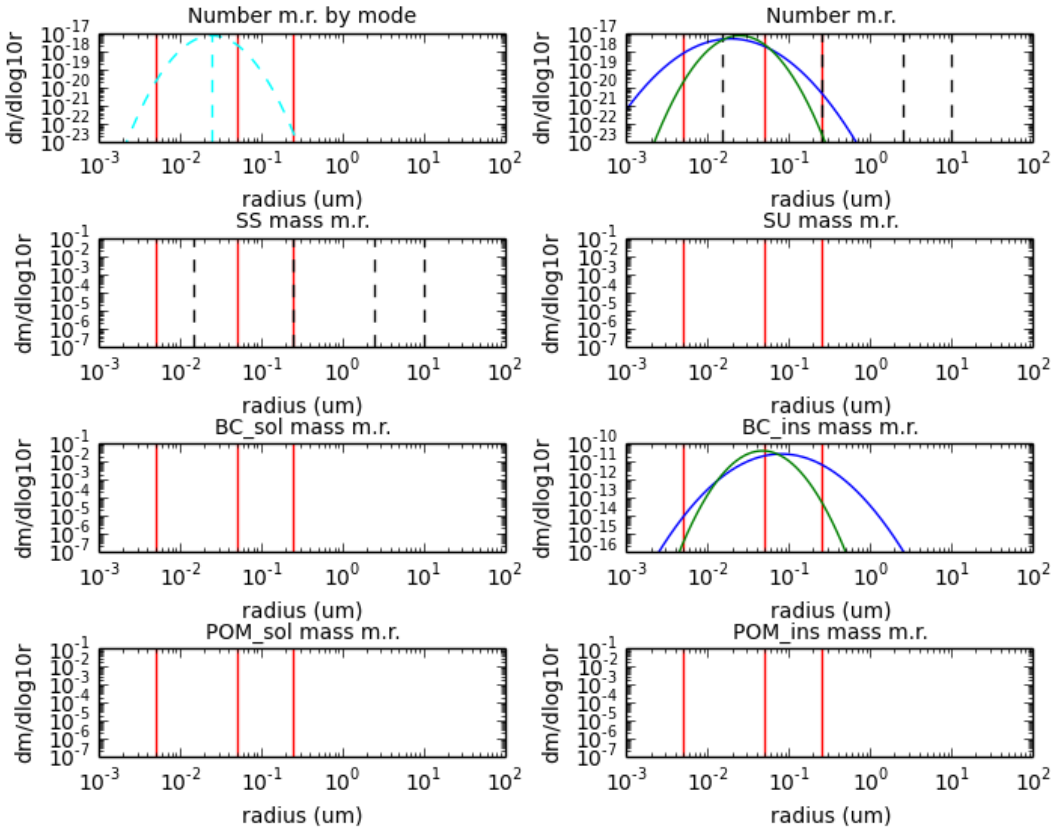

Figure 3d. C-IFS distributions (blue) and the corresponding GLOMAP-mode distributions (green) for **'Hydrophobic BC only'** C-IFS test record. Black dotted lines show C-IFS bin boundaries. Red lines show GLOMAP mode boundaries. Top left: Number distributions for individual GLOMAP modes (blue = Nucleation Mode, cyan = Aitken Mode, green = Accumulation Mode, black = Coarse Mode; dotted line indicates the insoluble Aitken mode). The geometric mean radius for each mode is shown by a vertical line.

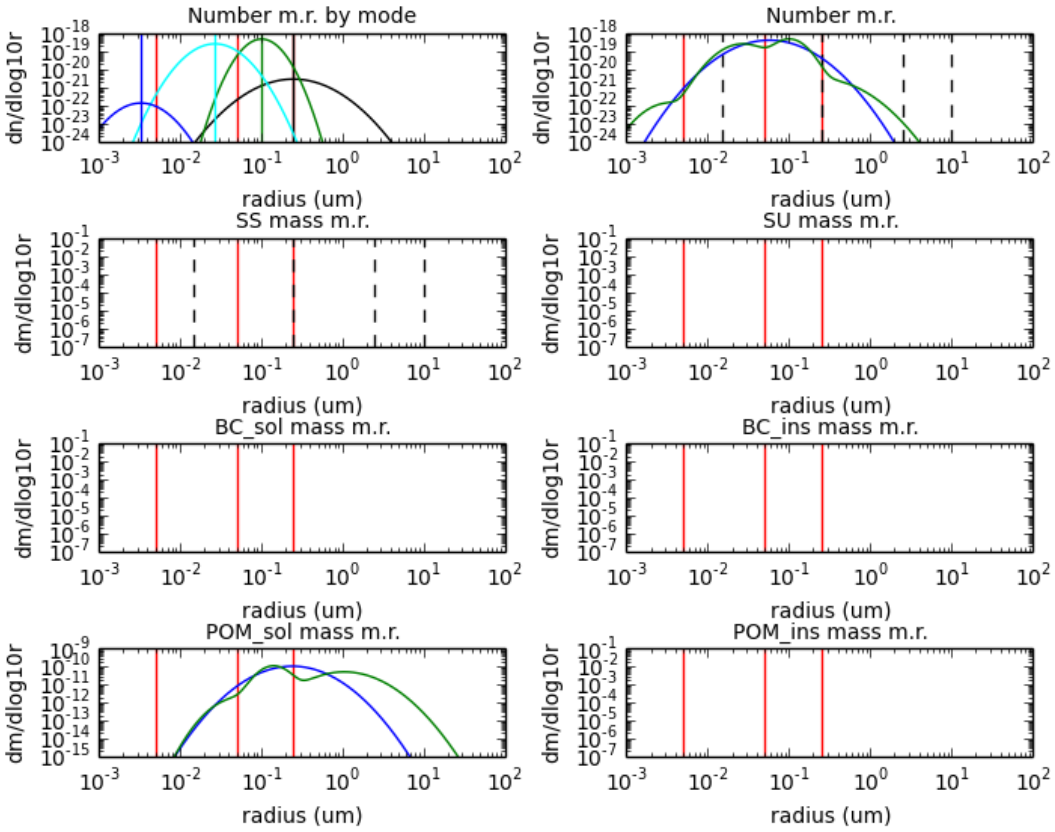

Figure 3e. C-IFS distributions (blue) and the corresponding GLOMAP-mode distributions (green) for **'Hydrophilic POM only'** C-IFS test record. Black dotted lines show C-IFS bin boundaries. Red lines show GLOMAP mode boundaries. Top left: Number distributions for individual GLOMAP modes (blue = Nucleation Mode, cyan = Aitken Mode, green = Accumulation Mode, black = Coarse Mode; dotted line indicates the insoluble Aitken mode). The geometric mean radius for each mode is shown by a vertical line.

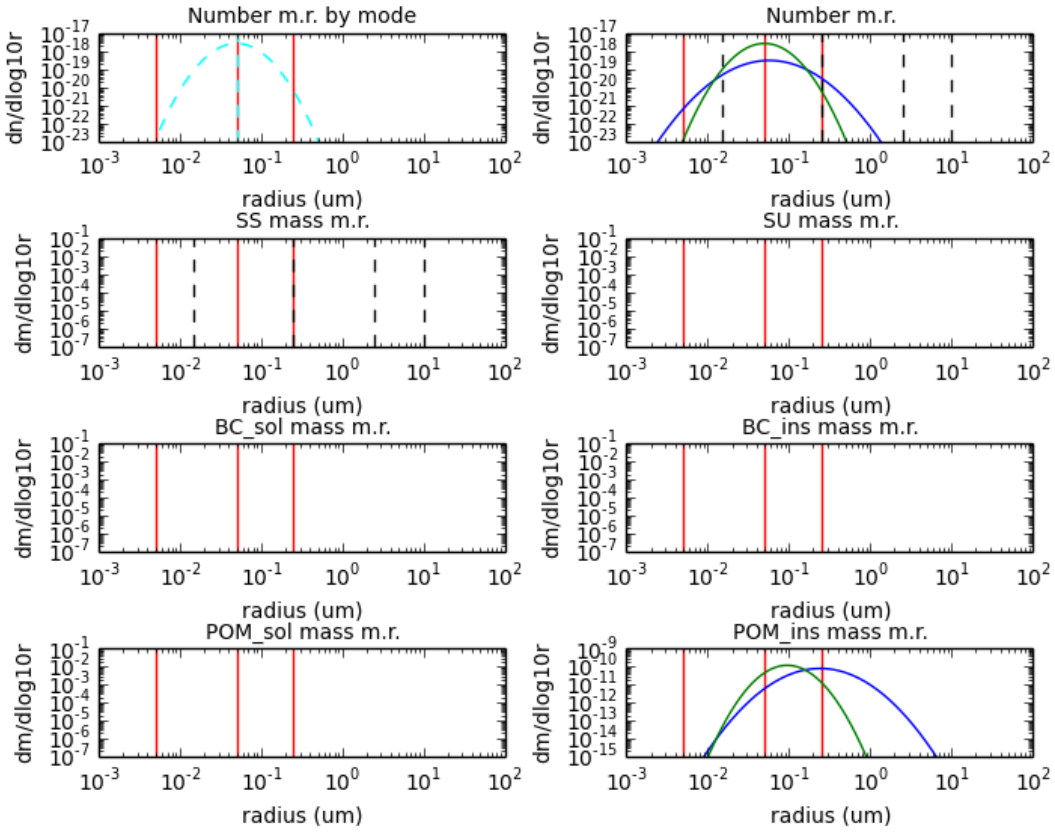

Figure 3f. C-IFS distributions (blue) and the corresponding GLOMAP-mode distributions (green) for **'Hydrophobic POM only'** C-IFS test record. Black dotted lines show C-IFS bin boundaries. Red lines show GLOMAP mode boundaries. Top left: Number distributions for individual GLOMAP modes (blue = Nucleation Mode, cyan = Aitken Mode, green = Accumulation Mode, black = Coarse Mode; dotted line indicates the insoluble Aitken mode). The geometric mean radius for each mode is shown by a vertical line.

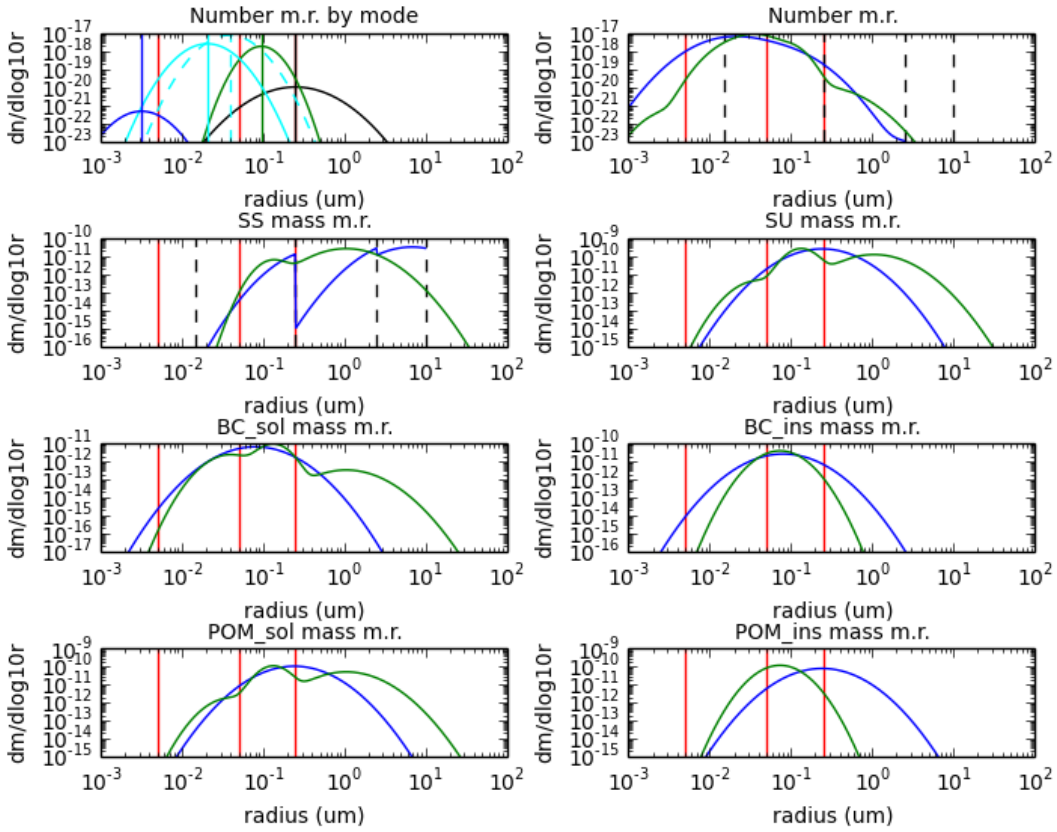

Figure 4a. C-IFS distributions (blue) and the corresponding GLOMAP-mode distributions (green) for **'Baseline'** C-IFS test record. Black dotted lines show C-IFS bin boundaries. Red lines show GLOMAP mode boundaries. Top left: Number distributions for individual GLOMAP modes (blue = Nucleation Mode, cyan = Aitken Mode, green = Accumulation Mode, black = Coarse Mode; dotted line indicates the insoluble Aitken mode). The geometric mean radius for each mode is shown by a vertical line.

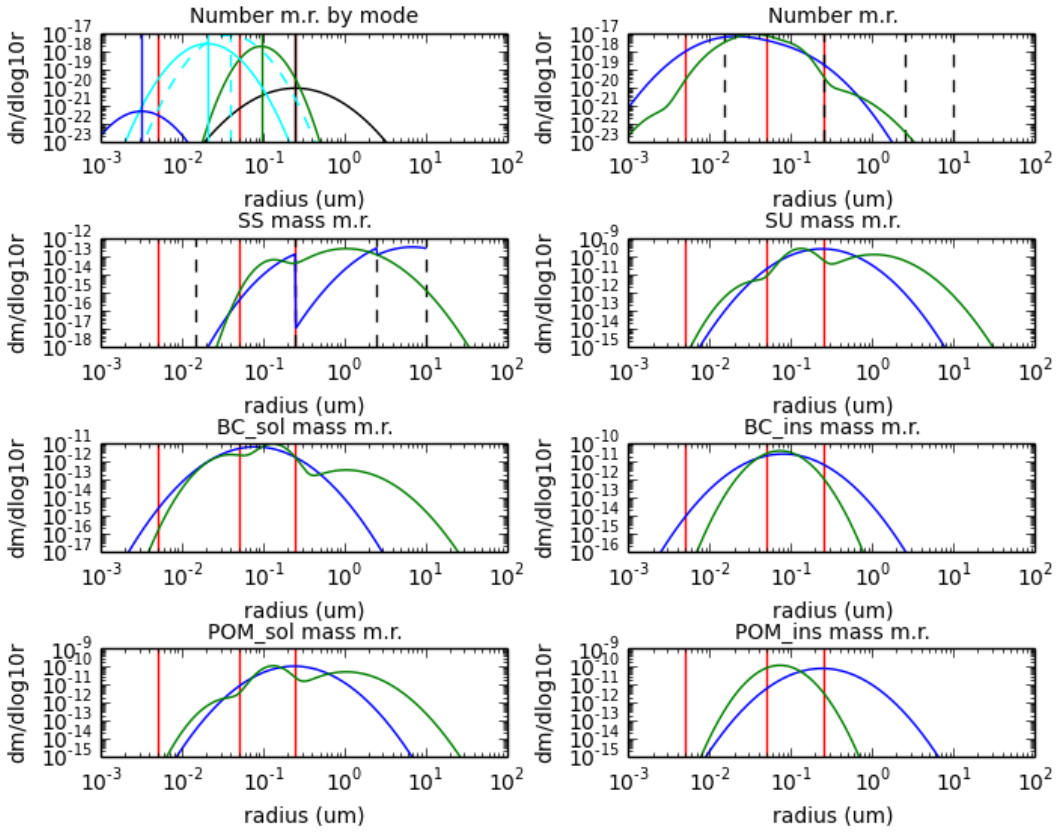

Figure 4b. C-IFS distributions (blue) and the corresponding GLOMAP-mode distributions (green) for **'Low SS'** C-IFS test record. Black dotted lines show C-IFS bin boundaries. Red lines show GLOMAP mode boundaries. Top left: Number distributions for individual GLOMAP modes (blue = Nucleation Mode, cyan = Aitken Mode, green = Accumulation Mode, black = Coarse Mode; dotted line indicates the insoluble Aitken mode). The geometric mean radius for each mode is shown by a vertical line.

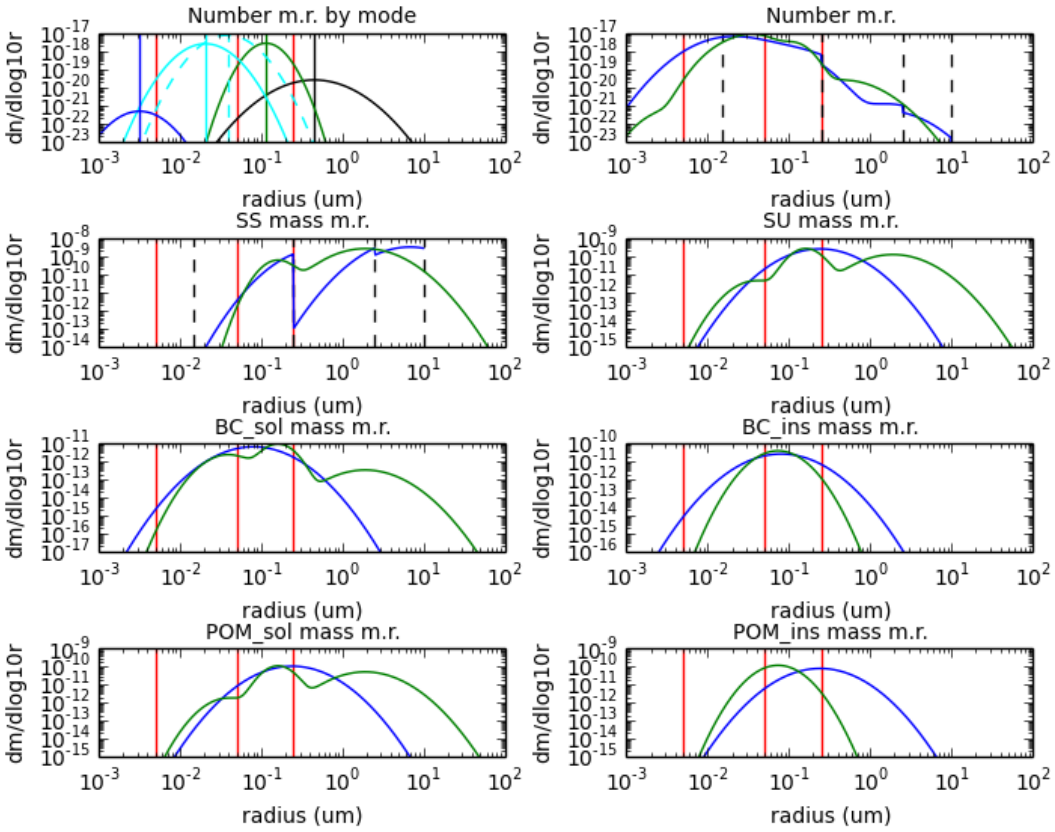

Figure 4c. C-IFS distributions (blue) and the corresponding GLOMAP-mode distributions (green) for **'High SS'** C-IFS test record. Black dotted lines show C-IFS bin boundaries. Red lines show GLOMAP mode boundaries. Top left: Number distributions for individual GLOMAP modes (blue = Nucleation Mode, cyan = Aitken Mode, green = Accumulation Mode, black = Coarse Mode; dotted line indicates the insoluble Aitken mode). The geometric mean radius for each mode is shown by a vertical line.

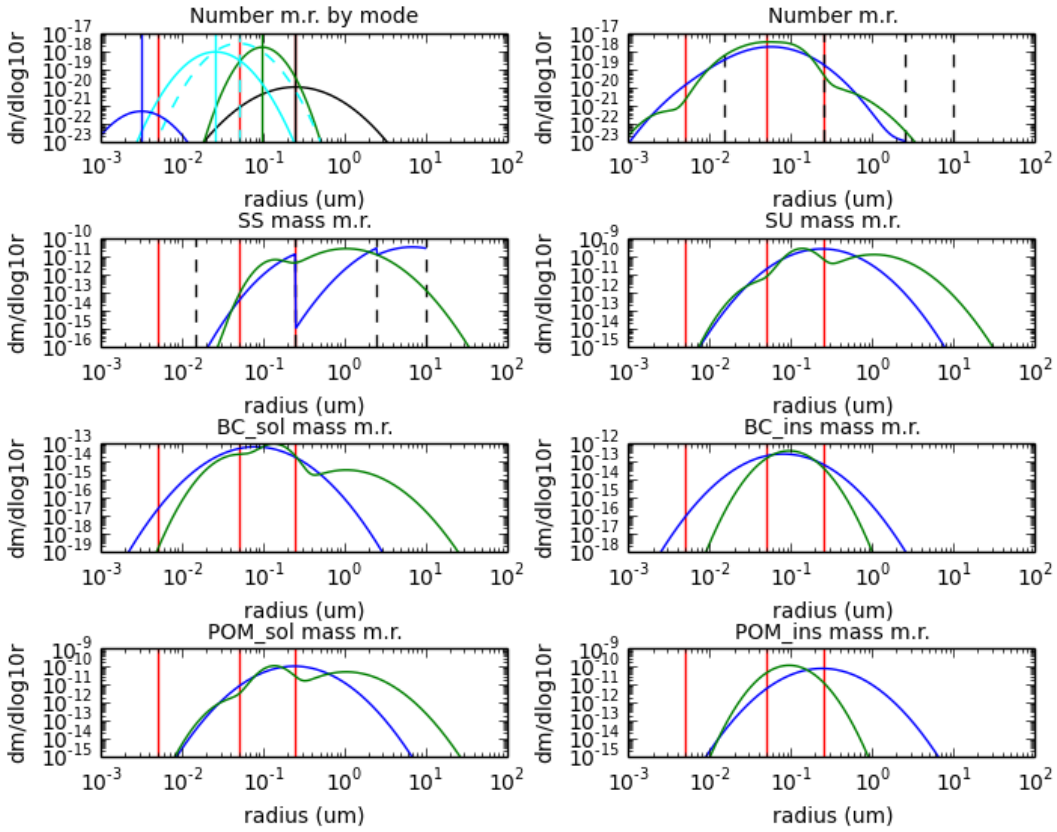

Figure 4d. C-IFS distributions (blue) and the corresponding GLOMAP-mode distributions (green) for **'Low BC'** an example C-IFS test record. Black dotted lines show C-IFS bin boundaries. Red lines show GLOMAP mode boundaries. Top left: Number distributions for individual GLOMAP modes (blue = Nucleation Mode, cyan = Aitken Mode, green = Accumulation Mode, black = Coarse Mode; dotted line indicates the insoluble Aitken mode). The geometric mean radius for each mode is shown by a vertical line.

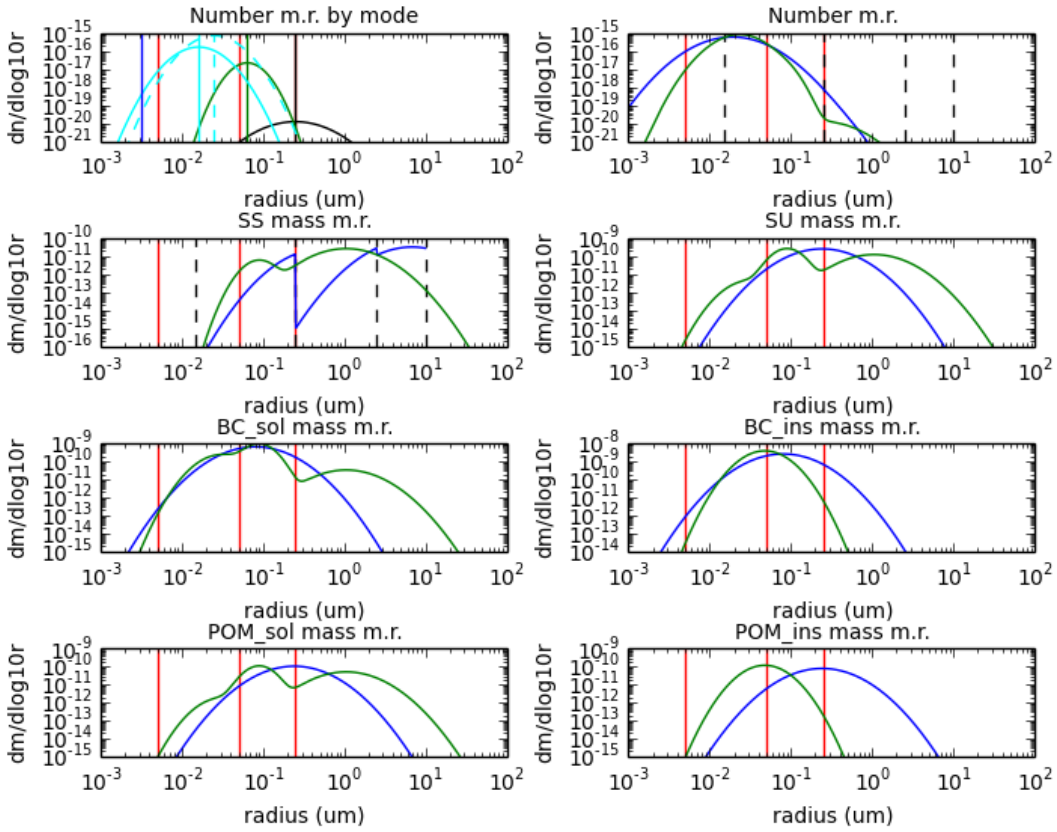

Figure 4e. C-IFS distributions (blue) and the corresponding GLOMAP-mode distributions (green) for **'High BC'** C-IFS test record. Black dotted lines show C-IFS bin boundaries. Red lines show GLOMAP mode boundaries. Top left: Number distributions for individual GLOMAP modes (blue = Nucleation Mode, cyan = Aitken Mode, green = Accumulation Mode, black = Coarse Mode; dotted line indicates the insoluble Aitken mode). The geometric mean radius for each mode is shown by a vertical line.

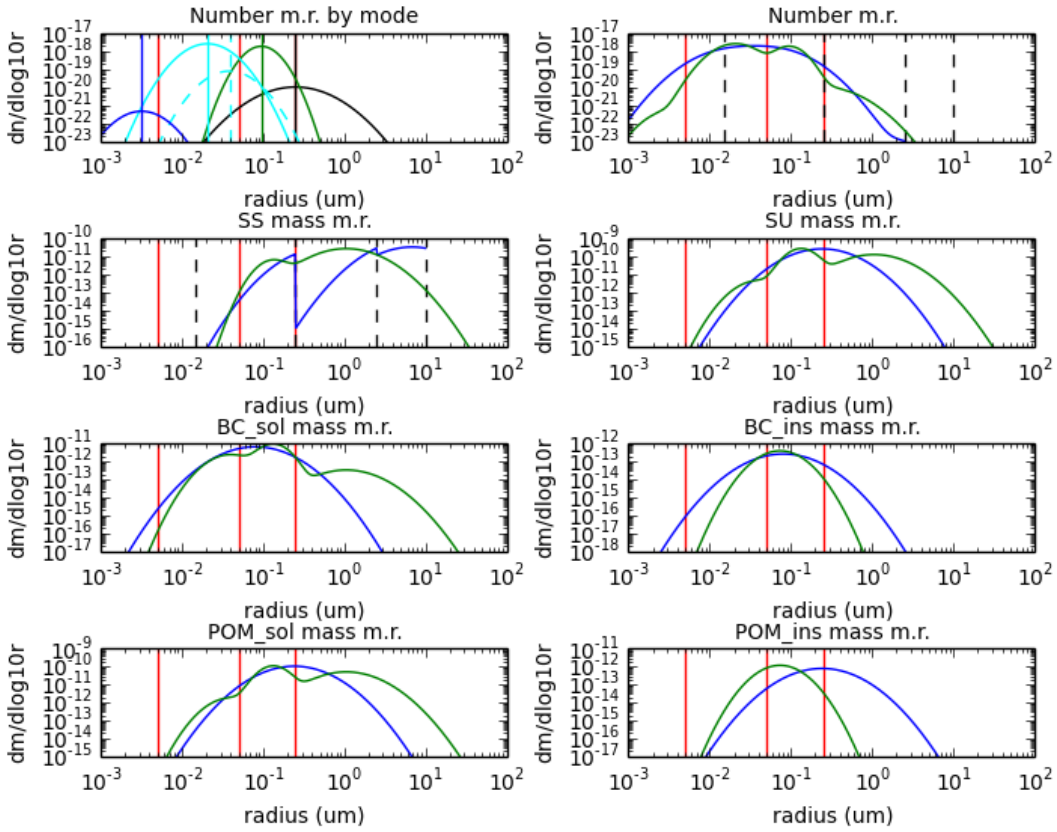

Figure 4f. C-IFS distributions (blue) and the corresponding GLOMAP-mode distributions (green) for **'Low Hydrophobic'** C-IFS test record. Black dotted lines show C-IFS bin boundaries. Red lines show GLOMAP mode boundaries. Top left: Number distributions for individual GLOMAP modes (blue = Nucleation Mode, cyan = Aitken Mode, green = Accumulation Mode, black = Coarse Mode; dotted line indicates the insoluble Aitken mode). The geometric mean radius for each mode is shown by a vertical line.

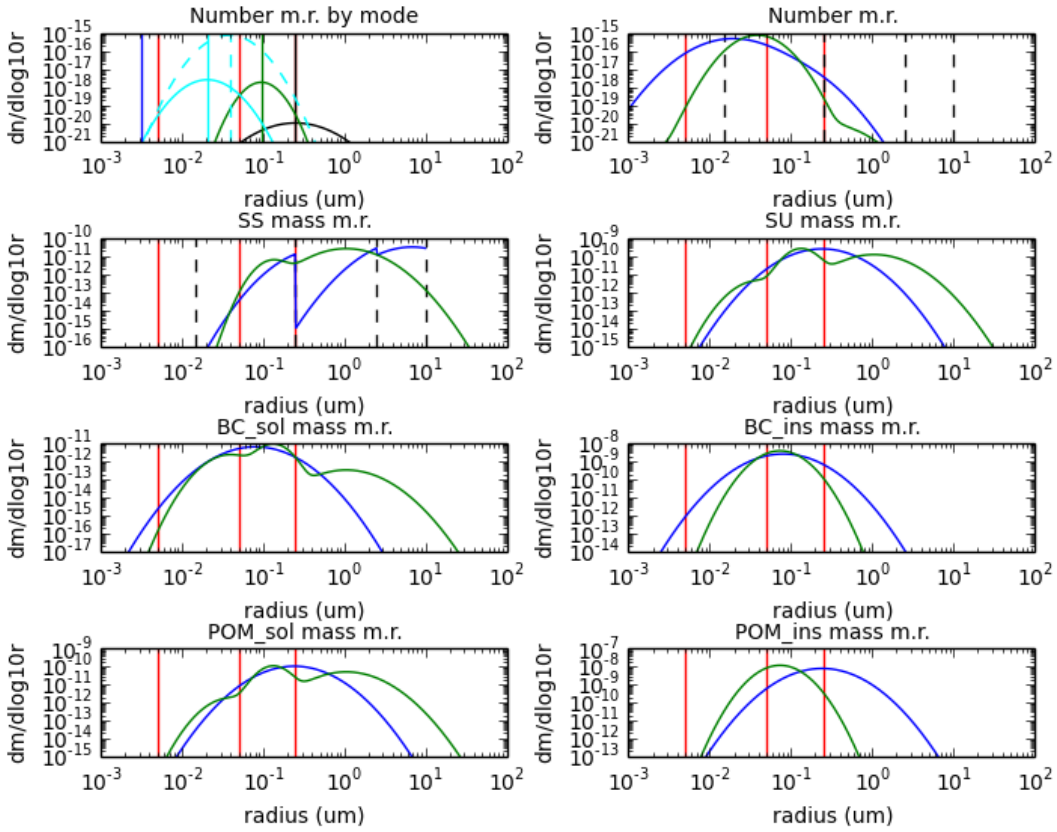

Figure 4g. C-IFS distributions (blue) and the corresponding GLOMAP-mode distributions (green) for **'High Hydrophobic'** C-IFS test record. Black dotted lines show C-IFS bin boundaries. Red lines show GLOMAP mode boundaries. Top left: Number distributions for individual GLOMAP modes (blue = Nucleation Mode, cyan = Aitken Mode, green = Accumulation Mode, black = Coarse Mode; dotted line indicates the insoluble Aitken mode). The geometric mean radius for each mode is shown by a vertical line.

References

Boucher and Anderson, 1995. J. Geophys. Res., 100, 26,117– 26,134.
Boucher et al., 2002. Note Sci. IPSL 23, 27 pp., Inst. Pierre Simon Laplace, Paris.
Fitzgerald, 1975. J. Appl. Meteorol., 14, 1044-1049.
Köpke et al., 1997. Tech. Rep. 243, pp. 103-158, Max-Planck-Inst. für Meteorol. Hamburg.
Mann et al., 2010. Geosci. Model Dev. 3, 519-551.
Mann et al., 2012. Atmos. Chem. Phys., 12, 4449–4476.
Morcrette et al., 2009. J. Geophys. Res. 114, D06206.
O' Dowd et al., 1997. Atmos. Environ. 31, 73-80.
Reddy et al 2005. J. Geophys. Res. 110, D10S16.

Met Office
FitzRoy Road, Exeter
Devon EX1 3PB
United Kingdom

Tel (UK): 0370 900 0100 (Int): +44 1392 885680
Fax (UK): 0370 900 5050 (Int): +44 1392 885681
enquiries@metoffice.gov.uk
www.metoffice.gov.uk